ELSEVIER

Palaeogeography, Palaeoclimatology, Palaeoecology 168 (2001) 141–169

PALAEO

www.elsevier.nl/locate/palaeo

The Abad composite (SE Spain): a Messinian reference section for the Mediterranean and the APTS

F.J. Sierro[a,*], F.J. Hilgen[b], W. Krijgsman[c], J.A. Flores[a]

[a]*Department of Geology, University of Salamanca, 37008, Salamanca, Spain*
[b]*Department of Geology, Faculty of Earth Sciences, Utrecht University,Utrecht, The Netherlands*
[c]*Paleomagnetic Laboratory "Fort Hoofddijk", Utrecht University,Utrecht, The Netherlands*

Received 7 July 1999; accepted for publication 28 August 2000

Abstract

A high-resolution integrated stratigraphy is presented for the Abad marls of the Sorbas and Nijar basins in SE Spain (pre-evaporitic Messinian of the Western Mediterranean). Detailed cyclostratigraphic and biostratigraphic analyses of partially overlapping subsections were needed to overcome stratigraphic problems in particular encountered at the complex transition from the Lower to the Upper Abad. The resulting Abad composite section contains a continuous stratigraphic record from the Tortonian/Messinian boundary up to the transition to the Messinian evaporites of the Yesares Member. All together, 18 calcareous plankton events were recognized which were shown to be synchronous throughout the Mediterranean by means of detailed (bed-to-bed) cyclostratigraphic correlations. The magnetostratigraphy allowed the identification of the four magnetic reversals of chron C3An in the Upper Abad. Details in the sedimentary cycle patterns allowed the Abad composite to be astronomically calibrated. This calibration to the 65°N summer insolation curve of solution $La90_{(1,1)}$ yielded astronomical ages for all sedimentary cycles, calcareous plankton bioevents, ash layers and paleomagnetic reversals. Up to now, the Abad composite is the only astronomically well-calibrated section that provided a reliable cyclostratigraphy, magnetostratigraphy and calcareous plankton biostratigraphy. As such it will serve as a reference section both for the pre-evaporite Messinian in the Mediterranean as well as for the Messinian interval in the Astronomical Polarity Time Scale.

Keywords: Biostratigraphy; Magnetostratigraphy; Milankovitch; Planktonic foraminifera; Mediterranean; Messinian

1. Introduction

During the last decade, high-resolution biostratigraphic, magnetostratigraphic and cyclostratigraphic studies of marine sections in the central and eastern Mediterranean have provided an excellent chronostratigraphic framework for the late Neogene (Hilgen 1987; Langereis and Hilgen, 1991; Krijgsman et al., 1995, 1997). Detailed cycle pattern analysis have allowed these sections to be tuned to astronomical target curves, resulting in astronomical time scales for the Plio-Pleistocene (Hilgen 1991a,b; Lourens et al., 1996) and the late Miocene (Hilgen et al., 1995). During the late Messinian, however, restricted environmental conditions in the Mediterranean caused a widespread deposition of evaporites, preceeded by cyclic alternations of diatomites and marls (e.g. Tripoli Formation of Sicily). These

* Corresponding author. Tel.: +923-29-4497; fax: +923-29-4514.
E-mail address: sierro@gugu.usal.es (F.J. Sierro).

0031-0182/01/$ - see front matter
PII: S0031-0182(00)00253-4

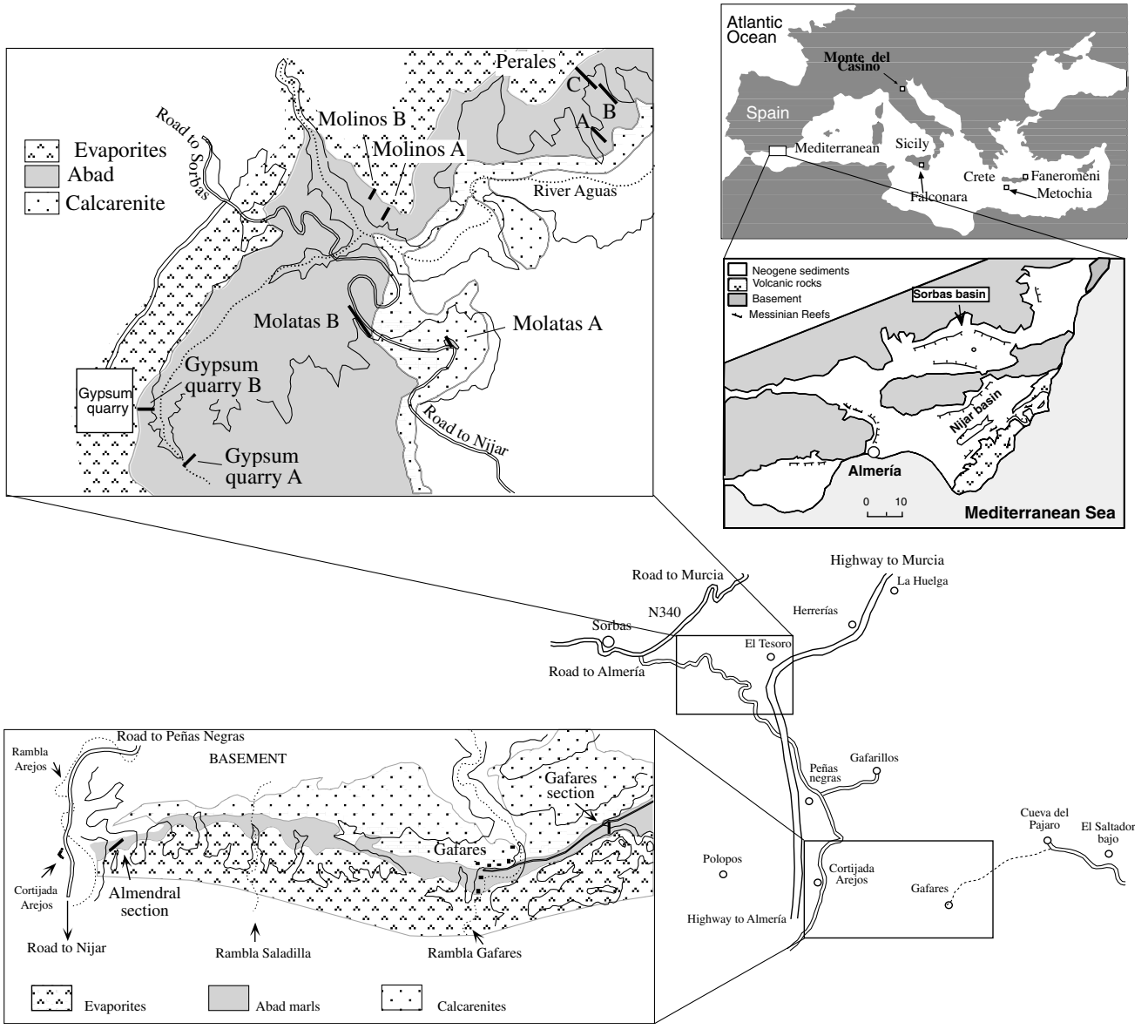

Fig. 1. Location map of the sections studied in this paper: (above) Sections of the Sorbas basin; and (below) Sections of the Nijar basin.

types of sediments are different from the hemipelagic deposits of Pliocene and early Messinian age and have until recently hindered the construction of an astronomical time (polarity) scale for the late Messinian.

Recently, it has been shown that the cyclic bedding of the pre-evaporitic diatomites is related to astronomically controlled variations in regional climate as well (Hilgen et al., 1995; Sprovieri et al., 1996b; Sierro et al., 1997, 1999; Krijgsman et al., 1999; Hilgen and Krijgsman, 1999; Vazquez et al., 2000). Up to now, however, no section has provided a reliable and continuous magnetostratigraphic record. Tripoli sections from Sicily reveal a secondary (overprinted) normal magnetisation (Langereis and Dekkers, 1992) or show controversial results (Gautier et al., 1994; McClelland et al., 1997). Sections in the Northern Apennines (Italy) are subject to diagenetic overprinting and strong tectonic deformation (Krijgsman et al., 1997; Negri and Vigliotti, 1997), while the Metochia diatomite section on Gavdos (Greece) is overprinted by a secondary reversed component (unpublished data).

To date, the Abad marls of the Sorbas and Nijar basins in Southeast Spain are the only cyclically-bedded stratigraphic unit in the Mediterranean that may provide a reliable magnetostratigraphy for the pre-evaporitic Messinian from the Tortonian–Messinian boundary to the base of the evaporites. Gautier et al. (1994) reported the first magnetostratigraphic data from the Sorbas basin, correlating the Abad marls to chrons C3Bn, C3Ar, C3An and C3r (Gilbert Chron) and the evaporites (Yesares member) to the lower part of chron C3r. The cyclostratigraphic potential of the Abad member was further evaluated by Sierro et al. (1997, 1999), showing that the sedimentary cyclicity was controlled by the astronomical precession cycle.

The Abad member is therefore suitable for establishing an astronomical polarity time scale (APTS) for the crucial period of time that heralds the onset of the Messinian salinity crisis (see Krijgsman et al., 1999). This study mainly focuses on the elaboration of an integrated stratigraphy for the Abad Member, which will be used to establish a standard chronostratigraphic framework both for the pre-evaporitic Messinian of the Mediteranean as well as for the late Messinian interval of the APTS.

2. General setting and stratigraphy

The Sorbas and Nijar basins (Fig. 1) are small Late Neogene depressions that evolved in the Eastern Betics (SE Spain) in a structural corridor that was subjected to compressional and extensional events (Montenat and Ott d'Estevou, 1996). During the late Tortonian, a general uplift caused an important sedimentary discontinuity in both basins (Weijermars et al., 1985; Martin and Braga, 1996), separating middle–upper Tortonian hemipelagic and turbiditic sediments from the uppermost Tortonian–lower Messinian pre-evaporitic deposits (Ott d'Estevou 1980; Van de Poel, 1991; Martin and Braga, 1996). The pre-evaporitic sequence starts with calcarenitic deposits of latest Tortonian age (*Azagador member*, Völk 1964), overlying the middle–upper Tortonian sediments or, unconformably, the basement. These calcarenites of the Azagador member rapidly grade upward into marls, clays and diatomites of early Messinian age, generally classified in the literature as the Abad member (Völk and Rondeel, 1964). The base of the Abad member usually consists of a yellowish silty unit of several meters thickness, which can be regarded as a transitional facies between the Abad and Azagador.

The Abad marls, deposited in relatively deep parts of the Sorbas and Nijar basins, usually interfinger and grade laterally and vertically into platform carbonates and reefs (*Cantera member*, Völk 1964) that grow along the margins in shallower waters (Dronkert and Pagnier, 1977; Ott d'Estevou, 1980; Dabrio et al., 1985; Martin and Braga, 1990, 1994, 1996; Braga and Martin, 1996). Several studies have identified an upward change, both in sedimentary facies and micropaleontologic content, allowing the Abad marls to be divided into two distinct units. (Geerlings 1977; Dronkert and Pagnier, 1977; Civis et al., 1979; Ott d'Estevou, 1980; Van de Poel, 1991; Sierro et al., 1997, 1999; Vazquez et al., 2000). The Lower Abad is characterised by an alternation of indurated homogeneous whitish marls and softer homogeneous grey marls rich in planktonic foraminifera. Grey-brownish laminated sediments, hereafter referred to as sapropels, are only interbedded in its uppermost part. The Upper Abad is recognised in the field by its brownish colour and is characterised by the intercalation of sapropels and indurated diatom-rich (diatomites) layers containing

more benthic foraminifera and plant remains. These diatomites are faintly laminated at the base and strongly laminated (paper shales) towards the top. Another characteristic of the Upper Abad is the intercalation of very thin laminae of distal sandy turbidites within the sapropels, indicating increasing grain-size in terrestrial input into the basins.

During deposition of the Lower Abad, sedimentation was continuous in most areas. However, the limit between the Lower and Upper Abad is marked either by a hiatus near the margins or by sediment instability, as evidenced by several slumps (multiple-slump event) that transported Lower Abad relicts into Upper Abad marls, deposited in the basin depocenters. The sedimentary instability was probably due to tectonic uplift of the basin margins, creating steep slopes that favoured sediment sliding into the deeper regions. In the Sorbas basin, the tectonic activity started during deposition of the upper part of the Lower Abad (i.e. from cycle LA17 upwards) but was intensified at the onset of the formation of the Upper Abad. This tectonic event might be the same as the one that caused a regional unconformity along the basinal margins (Martin and Braga, 1994, 1996). Messinian reefs of the Cantera member lie unconformably above the Azagador and lowermost Abad. This unconformity was caused by erosion of all, or part, of the Lower Abad along the basin margins and might have extended towards the basin centres, where sedimentation was only interrupted by the sliding of several repetitive slumps. A second slump is located in all Upper Abad sections of the Sorbas basin. This slump could be related to the unconformity that separates the bioherm unit from the fringing reef unit, two marginal facies of the Upper Abad according to Martin and Braga (1994, 1996).

The Abad marls have always been considered to be of early Messinian age and belong to the *Globorotalia mediterranea* and *Globigerina multiloba* subzones of D'Onofrio et al. (1975) (Iaccarino et al., 1975; Civis et al., 1979; Gonzales Donoso and Serrano, 1977; Van de Poel, 1991; Sierro et al., 1993). The base of the *G. mediterranea* subzone was recognized near the base of the Abad marls (Gonzales Donoso and Serrano, 1977; Sierro et al., 1993, 1996). The limit between the *G. mediterranea* and *G. multiloba* subzones was approximately correlated with the coiling change in *Neogloboquadrina acostaensis* that occurred in the middle part of the Upper Abad (Civis et al., 1979; Gonzales Donoso and Serrano, 1977; Geerlings, 1977; Van de Poel, 1991; Sierro et al., 1993; Gautier, et al., 1994). This latter event has been widely recognised throughout the Mediterranean below the Lower Evaporites, or the laterally equivalent Calcare di Base (Zachariasse, 1975; Colalongo, et al., 1979; Sprovieri, et al., 1996a,b). Furthermore, a general impoverishment of the microfauna is observed immediately preceding the evaporite deposition in the Mediterranean (D'Onofrio et al., 1975).

Both the Abad marls in the central part of the basins and the *Cantera* member along the margins are overlain by massive gypsum deposits with laminated pelitic intercalations (*Yesares member*, Ruegg 1964). The Yesares member is commonly correlated with the Lower Evaporites of the Central Mediterranean (Müller and Hsü, 1987; Gautier et al., 1994; Clauzon et al., 1996; Krijgsman et al., 1999), although some authors have proposed a correlation with the Upper Evaporites (Martin and Braga, 1994; Riding et al., 1998, 1999).

3. Sections studied

Four sections (Molatas, Molinos, Gypsum quarry, Perales) in the Sorbas Basin (Fig. 1) and two (Almendral, Gafares) in the Nijar Basin were studied to obtain a continuous and complete record of the Abad member, i.e. from the top of the calcarenites to the base of the evaporites.

3.1. Sorbas basin

The Molatas section is a composite of 2 subsections exposed along the old road from Sorbas to Nijar, between Km 6 and 7 on the southern side of the Rio Aguas (Fig. 1). Molatas A is a short subsection that covers the yellowish silts overlying the calcarenite and the lowermost part of the Abad marls. Molatas B extends from the top of the yellowish silts and comprises most of the Lower Abad (Fig. 4).

The Molinos section is located on the northern side of the Rio Aguas, 500 m north of Molatas, and also comprises two subsections. The base of Molinos A starts immediately above the multiple-slump event that marks the limit between the Lower and Upper Abad (Figs. 2 and 4). Several white indurated layers

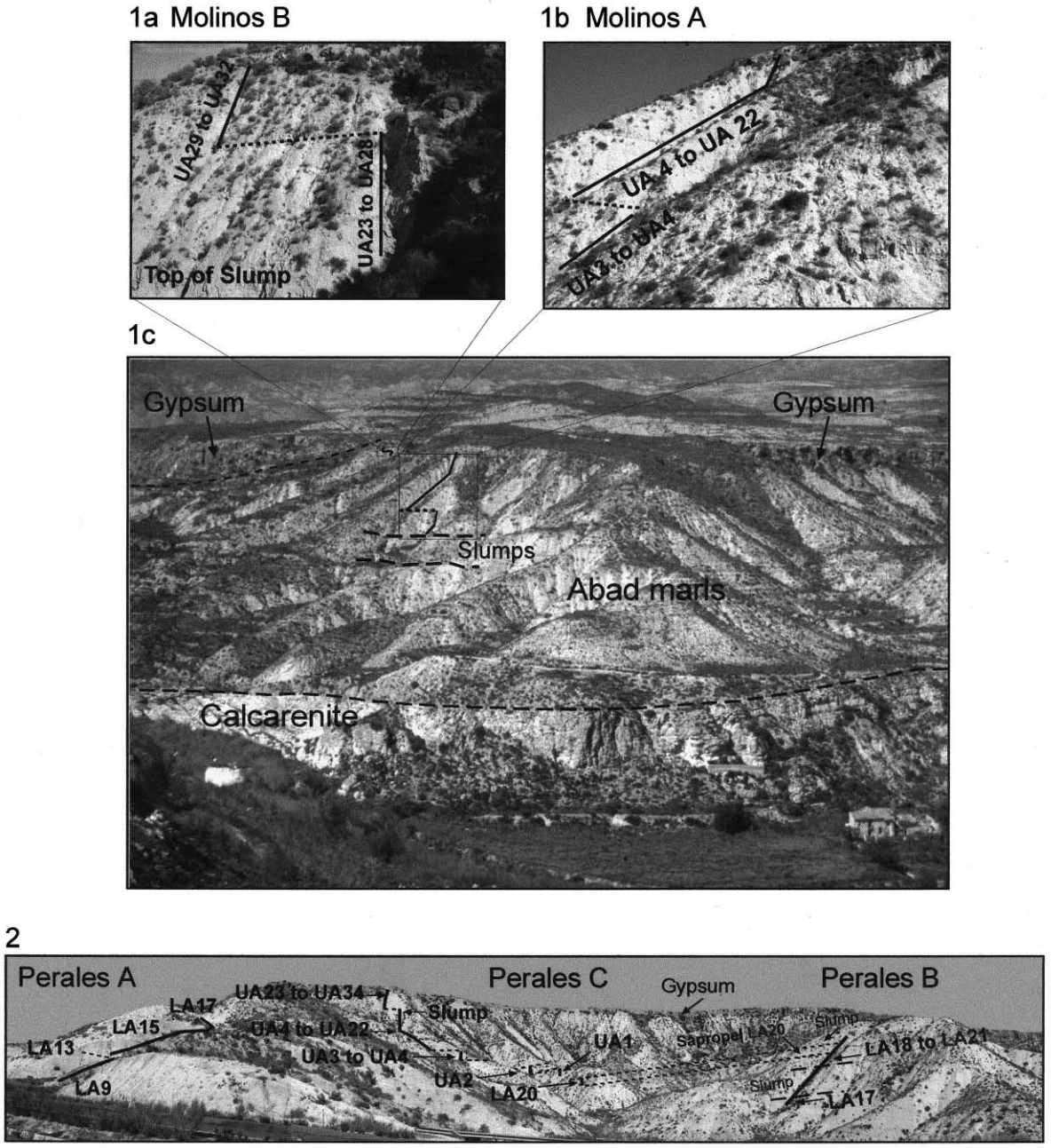

Fig. 2. Photographs of the Molinos subsections. 1c Panoramic wiew showing the calcarenites (Azagador member) at the base, the Abad marls in the middle and the Gypsum unit (Yesares member) on top. The location of subsections A and B is also shown. 1a and 1b: Pictures showing the sampling trajectories of subsections A and B and the cycles identified in every subsection. 2: Photograph showing the sampling trajectories of the Perales subsections A, B and C. The gypsum unit is on top of the hill.

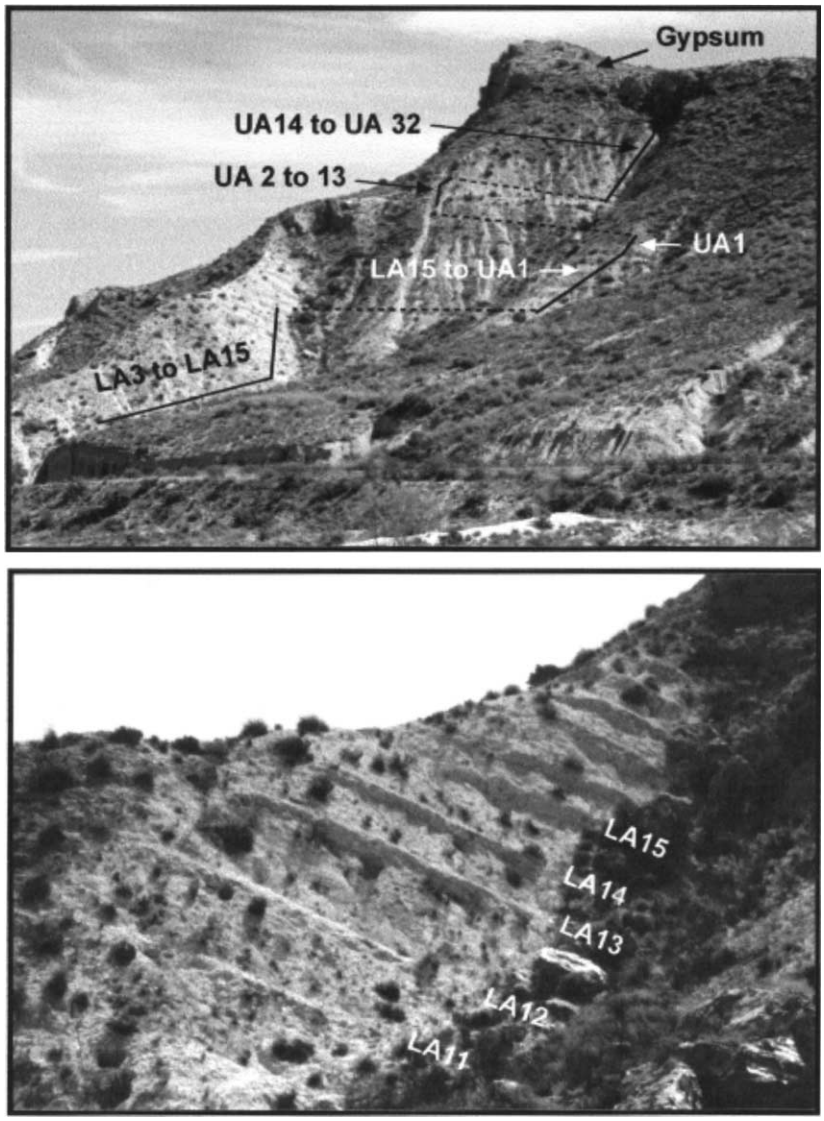

Fig. 3. Top: Photograph showing the sampling trajectories of the Gafares section indicating the different intervals by the cycle numbers. Bottom. Detailed picture of the Lower Abad in Gafares showing the characteristic alternation of indurated layers and homogeneous marls. Cycles LA11–LA15 were sampled in this gully.

are present in the lower part while thin, well-laminated diatomites (paper shales) occur towards the top. Because the upper part of this section was capped by Plio-Pleistocene conglomerates, we sampled Molinos B (next gully to the northwest, Fig. 2) to complete the uppermost part of the Upper Abad. It was possible to correlate both subsections by lateral tracing of some marker beds. We chose the distinct, 6.5 m thick, upper slump unit in the top part of Molinos A as the starting point of Molinos B. In the latter section, a few very prominent paper shales are clearly visible in the weathered outcrop. Unfortunately, the uppermost levels and the transition to the Gypsum are not well exposed.

The Gypsum quarry section consists of two subsections lying on both sides of a tributary of the Rio

Aguas, immediately to the east and southeast of the main gypsum quarry (Fig. 1). Gypsum quarry section A shows yellowish silts at the base, immediately above the top of the calcarenites (*Azagador member*). These silts gradually pass upward into grey marls, recording most of the Lower Abad (Fig. 4). In section B, the limit between the lower and Upper Abad is recorded by a sharp change in colour and lithology. The Upper Abad is almost complete but cycle bedding is not clearly visible in the exposures because of surface weathering. However, several prominent paper shales can be clearly distinguished in the upper part of the gullies below the gypsum. Two slump intervals were recognized: the first, of 1.5 m, is characterised by small-scale deformations in the first sapropel of the Upper Abad; the second is clearly visible in the upper part. Above the upper slump, prominent paper shales are slightly folded indicating tectonic deformation. Part of the succession, which contains two of the prominent paper shales, has even been tectonically doubled. This repetition was confirmed by means of a detailed comparison with the other Abad sections which provided an excellent high-resolution control on the cyclostratigraphy.

The Perales section is located on the northern side of the Rio Aguas, approximately 2 km north-east of the village of Los Molinos (Figs. 1 and 2). Perales A records part of the Lower Abad, while Perales B reveals the transition between the Lower and Upper Abad, recording the multiple-slump event that includes part of the Lower Abad in this section (Fig. 4). Two very thick and prominent sapropels that mark the base of the Upper Abad can easily be traced laterally along the different gullies (see Fig. 2), indicating that sedimentation continued in this part of the basin after each slump event. Perales C extends from top of the multiple-slump event to the base of the Evaporites. Although some small-scale deformation was observed near the base of Perales C, sedimentation was continuous.

3.2. Nijar basin

The Gafares section is located on the northern margin of the Nijar basin near the village with the same name, on the right side of the road from this village to El Saltador bajo (Fig. 1). In the Gafares section, most of the Lower Abad is perfectly exposed, showing the characteristic indurated layers (see Fig. 3). This is the only section in which sedimentation was continuous in the Lower to Upper Abad transition, showing no evidence for slumping or hiatuses. The section has been extended to the base of the evaporites but the uppermost part is not well exposed and shows clear indications of tectonic deformation.

The Almendral section is found approximately 5 km west of Gafares. It covers most of the Lower Abad and the lower part of the Upper Abad (Fig. 4). The limit between the Lower and Upper Abad is very sharp, suggesting the existence of a hiatus. Both the indurated layers as well as some thick sandstone layers in the lower part of the section are clearly visible. Sapropels are already present in the Lower Abad but they are grey in colour. The Upper Abad cyclicity is evident but the identification of several shear planes parallel to the bedding prevented us from being certain about the cycle correlations. The Almendral section is overlain by Plio-Pleistocene conglomerates. Some paper shales are visible near the top. Many small faults are present but individual layers can readily be traced.

4. Cyclostratigraphy and tephrastratigraphy

In the Lower Abad sedimentary cycles are defined by the cyclic occurrence of indurated layers intercalated within the homogeneous marls (see Fig. 4). These indurated layers are between 20 and 60 cm thick and are usually characterised by abundant Opal Ct (Sierro et al., 1997, 1999; Vazquez et al., 2000). Because there are no sapropels in most of the Lower Abad we used the bottom of the indurated layers as the lower limit of the cycles. Based on these criteria, we defined cycles LA1–LA21. In the Upper Abad, a sapropelitic layer appears in the middle part of the homogeneous marls between two consecutive indurated layers. We used the base of the sapropels to define the limits of the cycles to maintain the same criteria used in other Mediterranean sapropelitic sections. Cycles UA1–UA34 were recognized in the Upper Abad. Because of this change in the denomination of the cycles between the Lower and Upper Abad, cycle LA21 and cycle UA1 are partially the same (see Fig. 4).

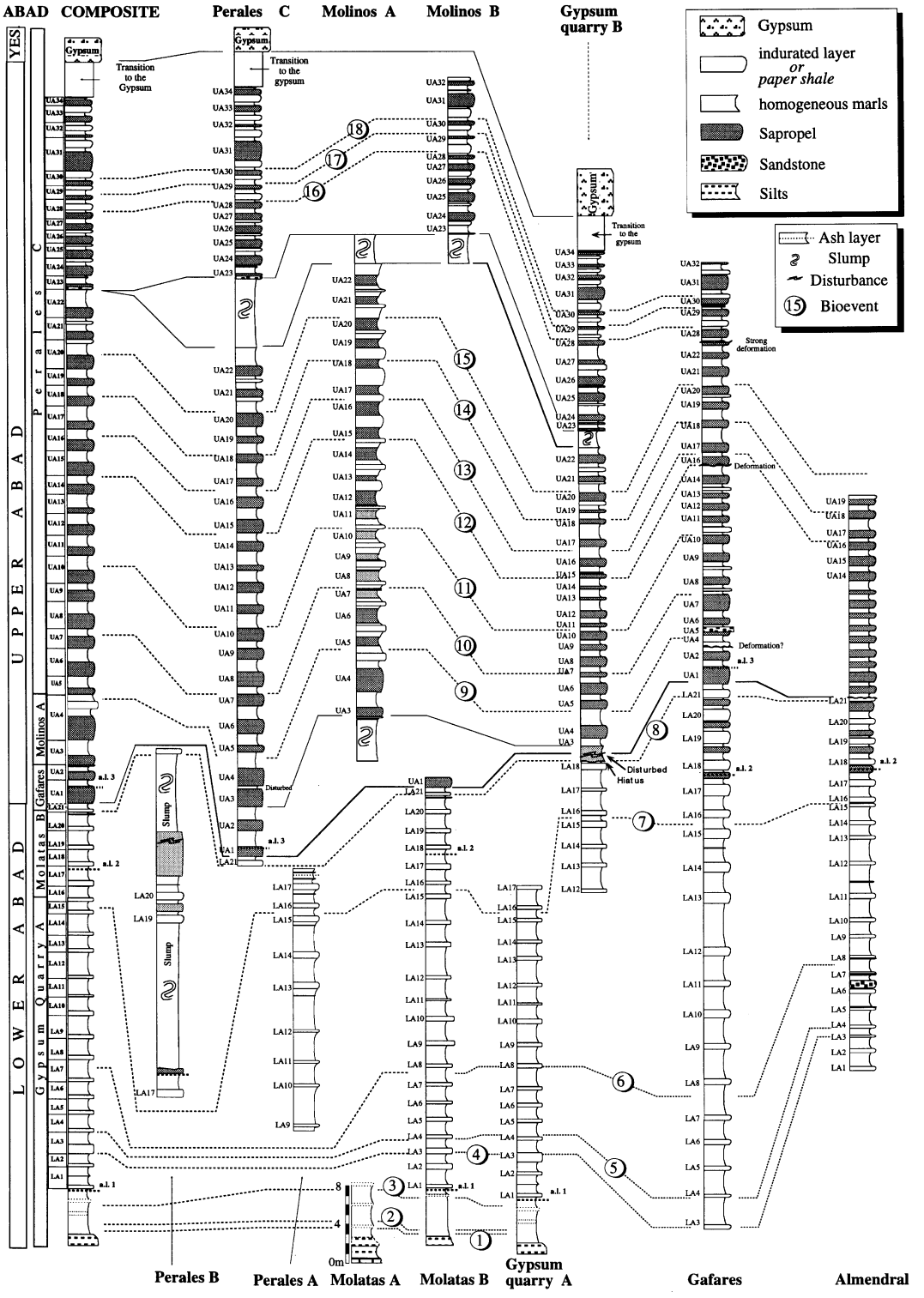
ABAD COMPOSITE
Perales C
Molinos A
Molinos B
Gypsum quarry B
Gypsum
indurated layer or paper shale
homogeneous marls
Sapropel
Sandstone
Silts
Ash layer
Slump
Disturbance
Bioevent
Transition to the Gypsum
Transition to the gypsum
Strong deformation
Deformation
Deformation?
Disturbed Hiatus
Disturbed
Slump
a.l. 1
a.l. 2
a.l. 3
LOWER ABAD
UPPER ABAD
YESO
Perales C
Molinos A
Gafares
Molatas B
Gypsum Quarry A
Perales B
Perales A
Molatas A
Molatas B
Gypsum quarry A
Gafares
Almendral

In the lowermost part of the Abad, immediately above the yellow silts, cyclicity is not evident, although some sections (e.g. Molatas A and Gypsum Quarry A) show indications of slightly more indurated layers alternating with homogeneous marls (Fig. 4). Cyclicity starts to be clearly discernible with the occurrence of a first prominent indurated layer that lies several metres above the base of the marls. Because this is the first well distinguishable lithological cycle in all sections, we termed it as Abad Cycle 1 (LA1) (Fig. 5a). It is followed by cycles LA2, 3 and 4, which are usually thinner than normal. In the Sorbas basin, indurated layers of LA9 and LA10 are always prominent, in contrast to indurated layer 11, which is usually thin. In the Nijar basin, this pattern is less clear. Cycle LA12 is the thickest cycle, both in the Sorbas and Nijar basins. The homogeneous marls of cycle LA15 is always extremely thin and the homogeneous marls of cycle LA16 is also less thick than in most other cycles. The characteristic pattern of cycle LA15 and LA16 provides one of the most useful criteria for cyclostratigraphic correlations in the Lower Abad (see Fig. 4). In the Nijar basin (Almendral and Gafares sections), the first sapropel occurs in the middle part of the homogeneous marls of cycle LA17. In the Perales section, which is probably located near the depocenter of the Sorbas basin, the first sapropel also occurs in cycle LA17. In more marginal settings (i.e. Molatas B), sapropels were not formed until cycle (UA1) (LA21).

In the Upper Abad, cycles UA6 and UA7 have distinct sapropels, while the sapropels of cycles UA5, UA9 and UA11 are poorly developed. Besides, cycle UA4 is much thicker than average. Higher in the succession, the very thin sapropel of LA13 and the thicker-than-average homogeneous bed of UA17 are characteristic. In the uppermost part, the sapropel of UA31 is a good marker because it is very thick and weakly laminated. In contrast, the sapropel of UA32 is usually thin. The cyclic sedimentation ends with cycle UA34, which is overlain by a transitional interval to the Gypsum, characterised by the presence of clays and limestones. The transition to the Gypsum is always poorly exposed and therefore cyclicity is not easily recognisable in the field.

Three biotite-rich levels were identified in our sections. The lowermost ash layer was found inmediately below the indurated layer of cycle LA1. The middle ash layer was found within LA17. On top of sapropel UA1 two thin ash layers of less than 0.5 cm thickness are separated by a 2 cm thick marl layer in section Perales, whereas up to 6 or 7 very thin biotite-containing ash layers are found in the correlative cycle in the Gafares section. These characteristic layers, together with the high-resolution biostratigraphy, were very useful for the correlation of the sections in the complicated multiple-slump interval.

5. Biostratigraphy

Biostratigraphy was mainly based on quantitative and qualitative changes in the planktonic foraminiferal assemblages (Figs. 5 and 6) although some nannofossil results are presented as well.

5.1. Keeled globorotaliids

The groups of *Globorotalia menardii* (dex.) and *Globorotalia miotumida* (sin.) that play a keyrole in Mediterranean and Atlantic correlations were identified in all our sections. Specimens of *G. menardii* dex were only found in the lowermost samples of the Abad marls, inmediately above the top of the transitional yellowish silts (Figs. 4 and 5). The last occurrence (LO) of this group is followed 50 cm upward by the first regular occurrence (FRO) of the *Globorotalia miotumida* group (Figs. 4 and 5). Both groups do not coexist in our sections.

Fig. 4. Cyclostratigraphic and biostratigraphic correlations of all sections studied in this paper. 1. LO of the of the group of G menardii dex. 2. FrO of the *G. miotumida* group. 3. Influx of the highly conical forms of the *G. miotumida* group. 4. Top of the paracme of *R. pseudoumbilicus.*5. LAO of the group of *G. scitula* sin. 6. Strong reduction of the group of *G. scitula* dex. 7. Bottom acme of the group of *G. scitula* dex. 8. Top acme group of *G. scitula* dex. 9. FAO of *G. siphonifera*. 10. Last influx of the *G. miotumida* group. 11. LrO of the *G. miotumida* gr. 12. First abundant influx of *T. multiloba*. 13. Last abundant influx of sinistral Neogloboquadrinids. 14. First abundant influx of dextral Neogloboquadrinids. 15. Short influx of the group of *G. scitula* dex. 16. Influx sinistral Neogloboquadrinids. 17. Short influx of the group of *G. scitula* dex. 18. Influx. sinistral Neogloboquadrinids.

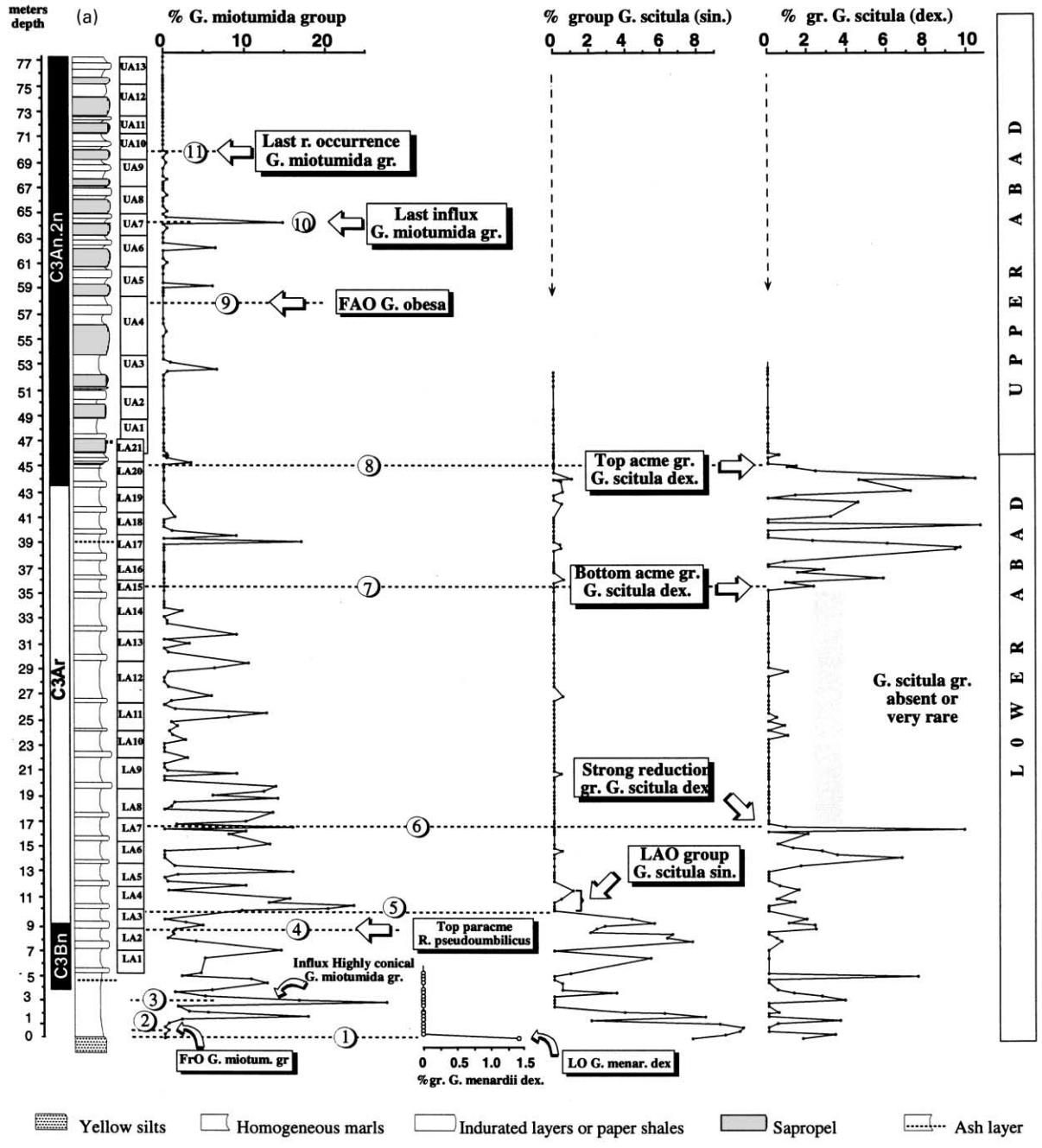

Fig. 5. Abundance variation of some of the planktonic foraminifera used to define the main bioevents. (a) From the base of the Abad marls to cycle A34. (b) From cycle A34 to the base of the Evaporites. Magnetostratigraphy from cycles 1 to 20 inferred from Krijgsman et al. 1995 and from cycles 20 to 55 based on this paper (see Fig. 7. This composite is based on the following sections: Molatas A, Molatas B, Molinos A and Molinos B. LA G. menar. dex. = Last occurrence of *Globorotalia menardii* dextral. FrO G. miotum. Gr. = First regular occurrence of the *Globorotalia miotumida* group. R. Pseudoumbilicus = Reticulofenestra pseudoumbilicus, LAO group G. scitula sin. = Last Abundance Occurrence of the group of *Globorotalia scitula* sinistral. Gr. G. scitula dex. = Group of *Globorotalia scitula* dextral. FAO G. obesa = First abundant occurrence of *Globigerina obesa*. Last r. Occurrence = Last regular occurrence. Percentage of the different taxa in relation to total planktonic foraminifera with the exception of the first column in 5b which shows the percentage of sinistral Neogloboquadrinids in relation to total Neogloboquadrinid.

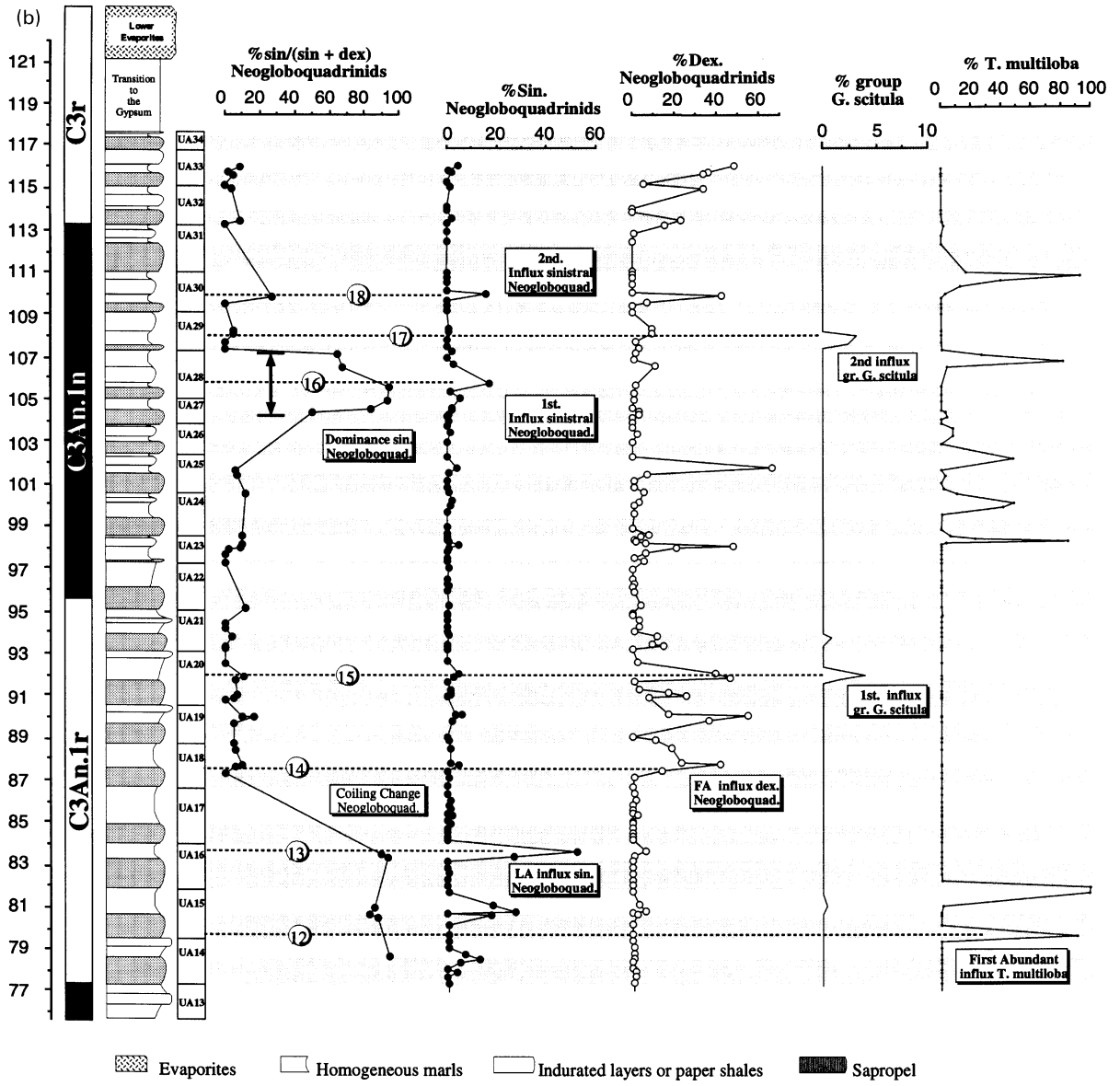

Fig. 5. (*continued*)

In the lower part, the *G. miotumida* group is dominated by less inflated forms (*G. miotumida* type), although highly conical types (*G. conomiozea*) may be very abundant in some of the younger levels. In particular, approximately 2 m below cycle LA1 a marked influx of highly conical forms was observed (Fig. 5a). This event was recognized in Molatas A, Molatas B and the Gypsum quarry sections (Fig. 4). The characteristic pattern of short incursions of the conical morphotype is also useful for biostratigraphic correlations. Furthermore, the group of *G. miotumida* shows strong periodic oscillations in abundance which can be used to mark, micropaleontologically, the precession cycles in the lower part of the Abad marls where the lithological cycles are not clearly visible (Fig. 5). The group is usually present during

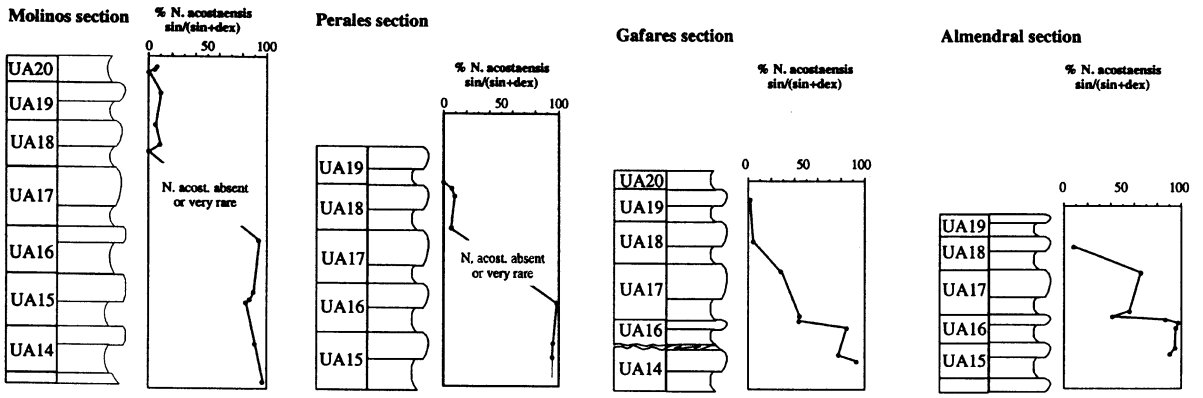

Fig. 6. Change in coiling direction from sinistral to dextral in the Neogloboquadrinids in the different sections.

deposition of the Lower Abad, but from cycle LA14 upward it shows a very irregular distribution with prominent incursions at specific levels that generally occur between the top of the sapropels and the base of the indurated layers (Fig. 5a). These incursions could be very useful for biostratigraphic correlations although a high sampling resolution is needed to confirm the presence or absence of these incursions in each cycle. The last two incursions are consistently recorded in cycles UA6 and UA7. From cycle UA7 upwards, the group of *G. miotumida* is scarce but present up to cycle UA10, where the last regular occurrence (LRO) of the group has been located in the study area (Fig. 5a).

5.2. Unkeeled globorotaliids

The distribution and coiling pattern of the unkeeled globorotaliids throughout the Messinian has proved to be very useful for biostratigraphic correlations both inside and outside the Mediterranean (Sierro et al., 1993; Krijgsman 1996; Krijgsman et al., 1995, 1997). The group of *Globorotalia scitula* (including *G. scitula* s.s., *G. suterae*, *G. nicolae*, *G. ventriosa*) is relatively abundant during the lower part of the Messinian and reveals frequent shifts in coiling direction, from sinistral to dextral and vice versa.

Sinistral forms, although with strong variations in abundance, are usually present with values over 4% of the total assemblage of planktonic foraminifera up to cycle LA 3, where their abundance is strongly reduced and indeed they almost completely disappear in the next cycle (Fig. 5a). This event was located in the Molatas, Gypsum quarry and Almendral sections. On the other hand, the group of *Globorotalia scitula* (dextral) is present at least up to the homogenous marls of cycle LA7, where they almost completely disappear as well. Between cycles LA8 and the homogeneous marls of LA15, an interval is recognised where the group, especially the sinistral forms, is almost completely absent.

From LA15–LA20, the *G. scitula* group is abundant again, but it is now dominated by the *G. nicolae* morphotype, with a preferentially dextral coiling (Fig. 5a). This interval has been named the Acme of the *G. scitula* (dex.) group. The form of *G. nicolae*, usually found in this interval, shows 4 or 4.5 chambers in the last whorl. In cycle LA20, *G. nicolae* is very abundant and has a very characteristic morphology with a strongly inflated ventral side, five or more chambers in the last whorl, and a very open umbilicus. The high abundance of this characteristic morphotype was very useful for cyclostratigraphic correlation, particularly for the identification of cycle LA20 in the multiple-slump interval between the Lower and Upper Abad in the Perales section. The top of the Acme of the *G. scitula* (dex.) group is marked by a sharp reduction of the group at the top of cycle LA20.

In the Upper Abad, unkeeled globorotaliids are almost completely absent with the exception of two short incursions (Fig. 5a). These events were identified in all sections in cycles UA20 and UA29. Another

minor peak of this group is observed in two sections in cycle UA9, but this peak has not been identified in the other sections.

5.3. Neogloboquadrinids

Neogloboquadrinids are abundant in most of the sections. A high-resolution quantitative study allowed us to recognise periodic fluctuations following the sedimentary cyclicity (Fig. 5b). Periodic fluctuations of sinistrally-coiled Neogloboquadrinids were recorded in most of the cycles up to cycle UA16, where we located the last abundant incursion of the sinistral forms of the group before the coiling change. From this cycle upward the sinistral Neogloboquadrinids become very rare, although two new incursions of sinistral Neogloboquadrinids were identified in the homogeneous layers of cycles UA28 and UA30 (Fig. 5b).

On the other hand the first prominent influx of dextral Neogloboquadrinids has been located in all sections on top of sapropel UA18. Between the homogeneous bed of UA16 and the top of sapropel UA18 Neogloboquadrinids are very scarce. To accurately locate the coiling change, a minimum of 50 specimens of Neogloboquadrinids was counted to calculate the ratio between the dextral and sinistral forms. As may be seen in Fig. 6, the dextral/sinistral ratio gradually changes along cycle UA17. This ratio is also very useful for the biostratigraphic correlation of the uppermost cycles. Above the first coiling change in cycle UA17, the Neogloboquadrinids are preferentially dextral with the exception of cycles UA27 (homogeneous) and UA28 in which the sinistral forms are dominant (Fig. 5b). Within cycle UA30, both dextral and sinistral forms are abundant with a *s/d* ratio around 30%.

5.4. Turburotalita multiloba influxes

The first occurrence of *T. multiloba* has been widely used for biostratigraphic correlations inside the Mediterranean. In the Sorbas and Nijar basins, the first two prominent incursions of *T. multiloba* were found near the base of UA15 and the transtion from UA15 to UA16 (Fig. 5b), i.e. 3.5 cycles below the first abundant incursion of the dextral Neogloboquadrinids. This species reveals characteristic cyclic variations in abundance that can at least be used for local biostratigraphic correlations.

5.5. Other ecostratigraphic events

Several peculiar changes in the planktonic foraminiferal assemblages were used for local biostratigraphic correlation, although some of them proved to be useful for correlations on a Mediterranean scale. A drastic reduction in planktonic foraminifera diversity was observed at the limit between the Lower and Upper Abad, approximately coinciding with the sharp reduction of the *G. scitula* (dex.) group. Diversity remains relatively high between LA1 and LA21 in the Lower Abad and falls dramatically within UA1 to values close to zero (see Sierro et al., 1999).

Intermediate specimens between *Globigerina obesa* and *Globigerinella siphonifera* are sometimes abundant in the Upper Abad. This species is scarce until the upper homogeneous marl of cycle UA4, where a prominent influx of this species was recognised. At this level, it reaches values over 60% of the total foraminiferal assemblage. This bioevent has been referred to as the FAO of *G. obesa* (Figs. 4 and 5) and is also abundant in other cycles of the Upper Abad.

Cycle UA13, characterized by a very thin sapropel, is one of the few cycles in this study that does not contain warm-oligotrophic foraminifera (see Sierro et al., 1999). *Globigerinoides* and *Orbulina* are usually the most abundant species in the sapropels, but are absent in the sapropel of cycle UA13. An interval characterised by a strong dominance of almost monospecific *Globigerina bulloides* extends from the top of the sapropel of cycle UA12 to the base of the sapropel of cycle UA14. This interval was found in the Perales, Molinos, Almendral and Gafares sections. Like sapropel UA13, the sapropel of UA31 is almost devoid of warm-oligotrophic planktonic foraminifera. This peculiar characteristic, together with the special lithology already described in the previous chapter, is very useful for cyclostratigraphic correlations in this part of the succession.

In the Upper Abad the number of planktonic foraminifera per gram of dry sediment fluctuates with a precession periodicity (see Sierro et al., 1999), whereby strong periodic reductions in the

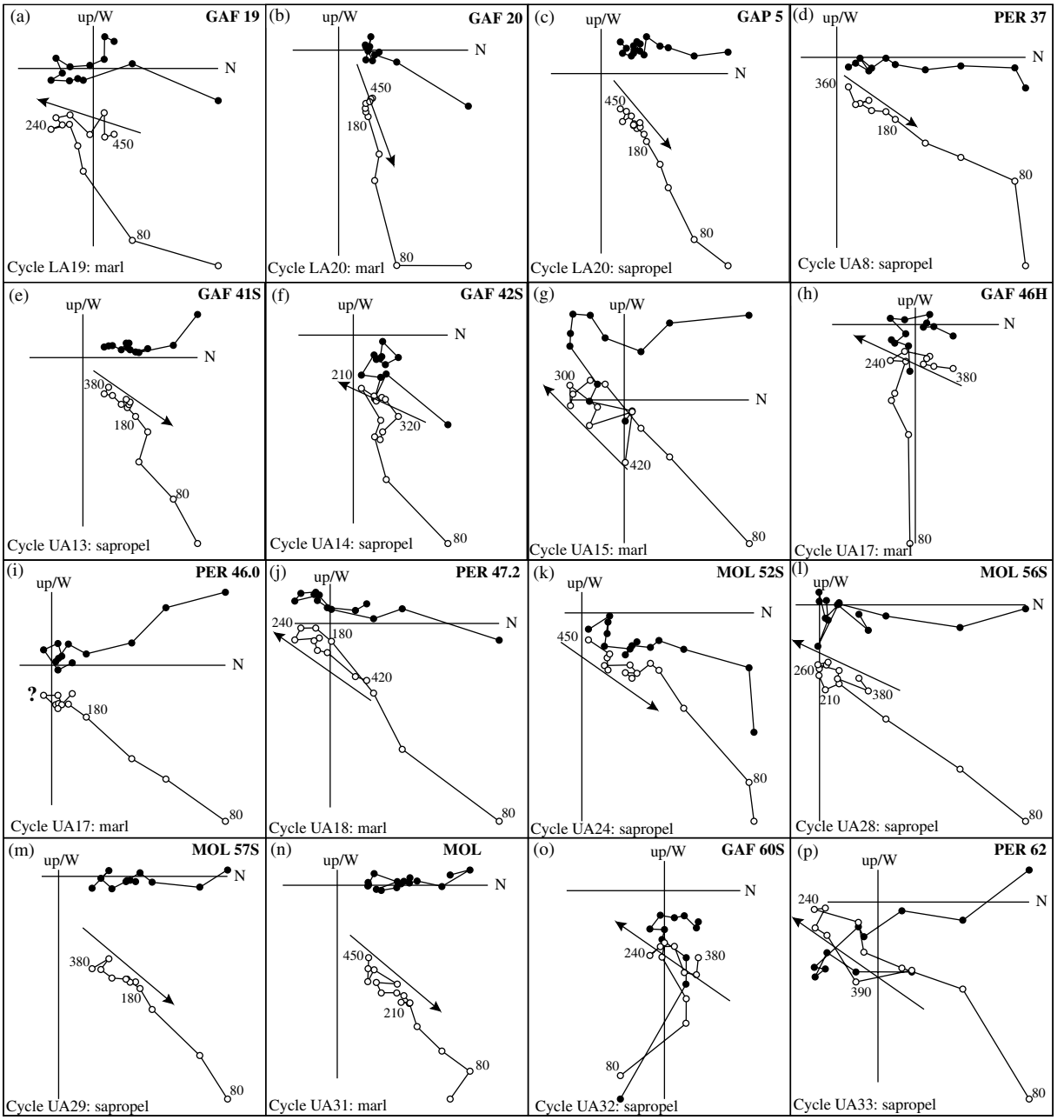

Fig. 7. Zijderveld demagnetisation diagrams of representative samples from the Gafares (GAF), Perales (PER), and Molinos (MOL) sections. All projections are in tectonic corrected coordinates. Closed (open) circles denote the projection on the horizontal (vertical) plane. Values represent temperatures in degrees Celsius. Cycle number and lithology are in the lower left corner. Type A samples only reveal normal polarities in the temperature range between 180 and 450°C. Type B samples are characterised by three NRM components. We have interpreted the reversed middle temperature (240–420°C) component as primary ChRM component.

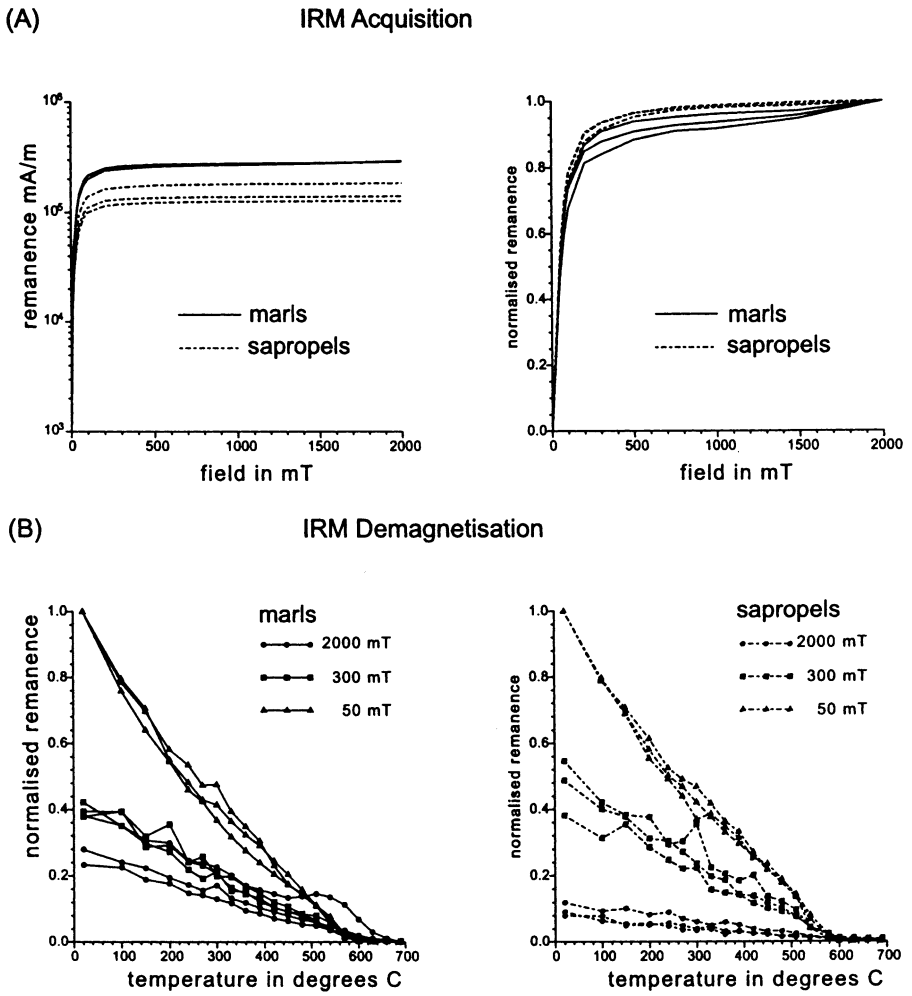

Fig. 8. (A) IRM acquisition curves of selected samples from marls and sapropels of the Gafares, Perales and Molinos sections. (B) Stepwise thermal demagnetisation diagrams of the normalised 3-axial IRM.

abundance of planktonic foraminifera occur near the transition from the homogeneous marls to the sapropels. This reduction, which has been recorded in most of the cycles of the Upper Abad, is more dramatic from cycle UA17 upwards, where short intervals almost devoid of planktonic foraminifera have been observed in the transitions between the homogeneous marls and the sapropels (Sierro et al., 1999). The pattern of periodic, temporal disappearances of planktonic foraminifera is first recorded in cycle UA17 in the Perales, Molinos, Almendral and Gafares sections.

5.6. Calcareous nannofossils

The calcareous nannofossil biostratigraphy of the Late Miocene is mainly based on discoaster and ceratolithid events but, unfortunately, both groups are scarce and show a discontinous distribution in the Abad marls. These shortcomings prevented to accurately define the position of these nannofossil events in our sections. However, a few specimens of *Amaurolithus amplificus* were observed between cycles LA20 and LA21.

By contrast, the reticulofenestrids have proved to be very useful for correlation with the global ocean.

From the base of the Lower Abad up to cycle LA2, *Reticulofenestra pseudoumbilicus*, with a maximum diameter larger than 7 μm, is absent or very rare. Above LA2 this species starts to be common.

6. Magnetostratigraphy

6.1. Sampling

In a first field trip, 137 levels were sampled in the Lower Abad marls of the Molatas B section, with a resolution of five levels per sedimentary cycle. At each level, we took standard paleomagnetic cores (25 mm diameter) using an electric drill and water as a coolant. Care was taken to remove the weathered surface. Thermal demagnetisation results from the Lower Abad showed that the paleomagnetic signal is very weak and strongly overprinted by a secondary normal component. Unfortunately, we were unable to obtain any reliable magnetostratigraphic data from these sediments, although Gautier et al. (1994) obtained good results from this interval. Contrary to us, Gautier et al. (1994) sampled the Molinos section and took oriented handsamples which he later drilled with air. During our second and third field trip we decided to employ the same sampling technique and to focus on the Upper Abad marls only. We took 37 samples in section Molinos, 62 in Perales, 26 in the Gypsum quarry, and 42 in Gafares, both from homogeneous marls as well as from sapropels. These handsamples were drilled with compressed air in the "Fort Hoofddijk" paleomagnetic laboratory.

6.2. NRM-demagnetisation

Natural remanent magnetisation (NRM) was measured on a 2G SQUID cryogenic magnetometer. All samples were thermally demagnetised, with small temperature increments of 20–30°C up to the level of inconsistent results. NRM intensities in both homogeneous marls and sapropels are relatively low, ranging between 0.05 and 0.02 mA/m. Unfortunately, 20% of the sampled levels showed diagrams that could not be interpreted reliably (Fig. 7i). Zijderveld diagrams of the other levels generally reveal two types of behaviour during thermal demagnetisation.

Type A samples only reveal normal polarities in the temperature range between 180 and 400–450°C (Fig. 7). At higher temperatures the paleomagnetic signal is generally too low to obtain reliable results and in some cases an additional viscous component is present. Zijderveld diagrams do not show a perfectly linear decay to the origin but a more scattered gradual decrease. This behaviour may be caused by a small residual field in the furnace in combination with the low intensities of the samples. Type A diagrams are dominant in the intervals of cycles LA20–UA13 and UA22–UA31 (Fig. 9). Type B samples are characterised by the presence of three NRM components (Fig. 7). A low-temperature component of normal polarity is removed in the temperature interval of 100–240°C; an intermediate-temperature component of reversed polarity is removed between temperatures of 240–420°C, and a high-temperature component of normal polarity is seen at temperatures above 420°C. This high-temperature component cannot be properly demagnetised because, as in the type A samples, no reliable signal can be recovered at temperatures higher than 450°C. Type B diagrams are dominant in the intervals of cycles LA18–LA19, UA14–UA21, and UA32–Gypsum (Fig. 9).

6.3. IRM-experiments

Acquisition of an isothermal remanent magnetisation (IRM) is indicative of the type of magnetic carrier. Low-coercivity minerals like magnetite are usually completely saturated at magnetic fields well below 300 mT, while high coercivity minerals such as hematite saturate at much higher fields. Subsequent thermal demagnetisation of the (saturation) IRM reveals the characteristic unblocking temperatures of the magnetic carriers. The IRM was acquired on selected samples from the homogeneous marls and from the sapropels. IRM acquisition curves show an initial steep rise until 100/200 mT, suggesting the presence of a low-coercivity mineral (Fig. 8a). Saturation is generally not reached in the highest fields (2000 mT), which indicates the additional presence of a high-coercivity mineral. The saturation IRM in the homogeneous marls is slightly higher than in the sapropels. The unblocking temperatures (570–600°C and 660–690°C) after thermal demagnetisation of the 3-axial IRM (Lowrie, 1990) support the presence of magnetite and hematite as the magnetic carriers

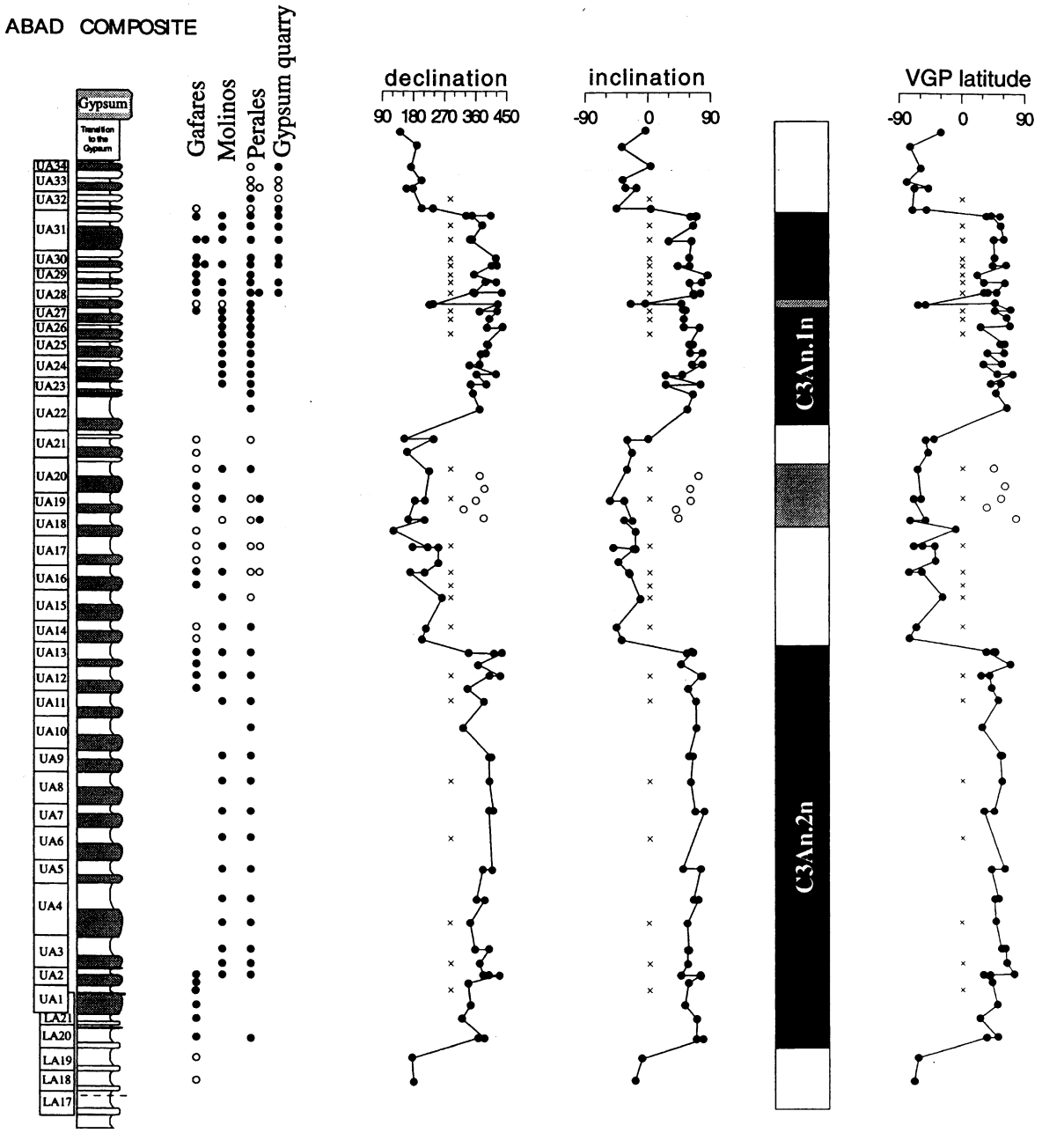

Fig. 9. Magnetostratigraphic data from the Abad composite. Closed symbols denote samples with a paleomagnetic signal sufficiently strong (0.01–0.1 mA/m) to determine the polarity. Open symbols denote directions interpreted as secondary overprint, crosses denote unreliable results.

(Fig. 8b). The contribution of hematite is negligible in the sapropels and small in the homogeneous marls as indicated by the high (2000 mT) field component of the demagnetisation curves.

6.4. Magnetostratigraphy

Thermal demagnetisation revealed the presence of three components of remanence, a low-temperature (100–240°C) normally directed component, an intermediate (240–420°C) dual polarity component, and a high-temperature (at least >420°C) normally directed component. The direction and the exact temperature range of the high-temperature component could not be determined because in many cases an additional viscous component was induced above 420°C and NRM intensities were generally too low to reliably interpret the demagnetisation diagrams. However, all high-temperature components show a normal polarity which strongly suggests that they are of secondary origin. Least-square analysis was applied to determine the low-temperature and intermediate component directions of the NRM (Kirschvink, 1980), chosen by inspection of vector end-point demagnetisation diagrams (Zijderveld, 1967). Mean directions were determined using standard Fisher statistics (Fig. 10).

The difference in bedding tilt between the Perales, Molinos and Gafares sections allows the application of a paleomagnetic fold test to differentiate between pre-folding and post-folding components. Fig. 10 shows that without tilt correction the section mean results of the low-temperature component are well-clustered with an inclination in agreement close to the present-day field value for the latitudinal position of the Sorbas/Nijar basin (inclination of 56°). Mean directions are divergent when tilt correction is applied, indicating that this low-temperature component is post-tilting and most likely related to (sub)recent weathering. The mean results of the intermediate component show a positive fold test because the scattered mean directions without tilt correction show a good clustering when tilt correction is applied. This indicates that the intermediate component is pre-folding and therefore we have interpreted it as the primary component.

Although a secondary overprint is dominant in all samples, reversed polarities are generally clearly revealed by stepwise thermal demagnetisation. Obviously, reversed polarities may be almost completely overprinted if weathering is intense. Especially the middle reversed interval shows several scattered samples with a normal polarity. But because samples from the same level in other sections reveal reversed polarities, we interpreted these normal polarities as secondary overprints. Another commonly observed overprint in cyclically-bedded, sapropel-bearing, sediments is "delayed acquisition" of the magnetic signal caused by diagenetic processes. For instance, Van Hoof et al. (1993) concluded that the high-temperature component in three-component diagrams from the cyclically-bedded Trubi marls was acquired later during early diagenesis, resulting from cyclically changing redox conditions within the sediment. The early Messinian polarity reversals of chron C3Bn are also found at different cyclostratigraphic positions, showing offsets of approximately one sedimentary cycle (Krijgsman et al., 1995, 1997). Delayed acquisition processes have also been put forwards as the most logical explanation for these discrepancies in polarity reversal ages, but the precise mechanisms are not yet established or fully understood. In the Abad marls, however, the high-temperature component is always of normal polarity and thus most likely related to sub-recent weathering processes and not to early diagenetic processes. Nevertheless, it cannot be excluded that such diagenetic processes have affected the 240–420°C component of the Upper Abad marls during NRM acquisition.

The interpretation of the intermediate component as the characteristic remanent magnetisation (ChRM) reveals five polarity zones in the interval studied (Fig. 9). We determined reversal boundaries: R/N between cycles LA19 and LA20; N/R between the homogeneous marls of UA13 and the sapropel of UA14, R/N between the homogeneous marls of UA21 and UA22, and N/R between the homogeneous marls of UA31 and the sapropel of UA32. We regard the consistency between all sections as an important argument for the validity of these intervals being of true normal and reversed polarity (Fig. 9).

7. Astronomical tuning of the Abad Composite

7.1. The Lower Abad

Our integrated cyclostratigraphic and biostratigraphic

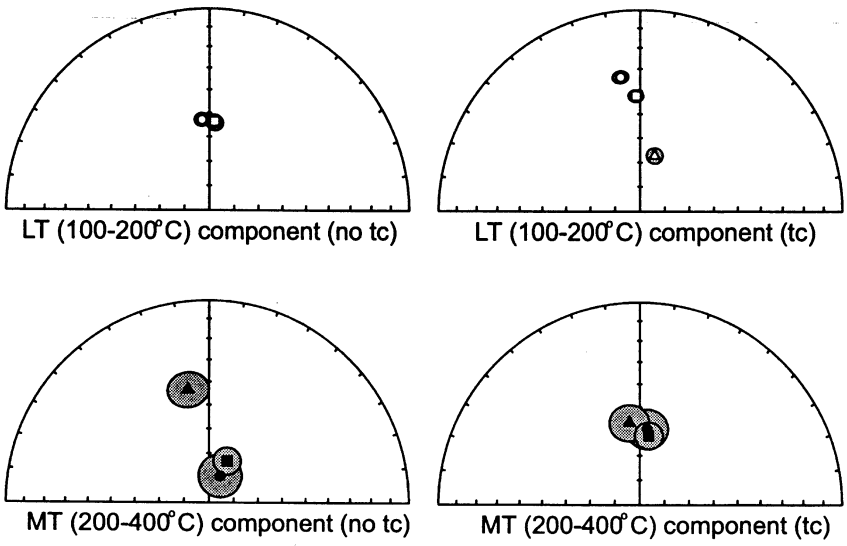

	section	N	Decl.	Incl.	Decl. (tc)	Incl. (tc)	k	a95
LT	Perales	46	355.2	52.8	352.3	33.3	56.6	2.8
	Molinos	33	3.3	53.4	358.6	42.2	85.6	2.7
	Gafares	39	3.6	54.2	15.9	66.4	51.4	3.2
	mean (no tc)	3	0.7	53.5	---	---	764.3	4.5
	mean (tc)	3	---	---	359.4	47.6	19.2	29.0
HT	Perales	34	23.0	78.3	5.5	59.1	9.8	8.3
	Molinos	18	24.0	71.6	7.6	61.8	40.4	5.5
	Gafares	27	349.5	42.7	352.7	56.5	14.1	7.7
	mean (no tc)	3	3.5	65.3	---	---	15.3	32.7
	mean (tc)	3	---	---	1.6	59.3	267.6	7.6

Fig. 10. Paleomagnetic fold test for the different NRM components in the Abad marls. Equal area projections of the site mean directions of the low-temperature (LT) and intermediate-temperature (MT) components from the Perales, Molinos and Gafares sections, before/after bedding tilt correction (no tc/tc) show that the LT component is post-tilting and the MT component is pre-tilting. Reverse directions are rotated 180° to antipodal. Directions of the high-temperature components could not be determined because in many cases an additional viscous component was induced above 420°C and NRM intensities were generally too low to reliably interpret the demagnetisation diagrams. Ellipses denote the 95% confidence regions around the mean directions. Table shows the statistical results: N = number of specimens; Decl, Incl. = section mean declination and inclination; k = Fisher's precision parameter; $\alpha 95 = 95\%$ cone of confidence.

data allowed an unambiguous correlation of the lower part of the Abad Composite (Lower Abad marls) to astronomically-dated sections in Italy and on Gavdos and Crete (Fig. 11) (Hilgen et al., 1995; Krijgsman et al., 1997). Because these sections have already been calibrated to astronomical target curves, all sedimentary cycles, bioevents and ash layers of the Lower Abad can be astronomically dated (Tables 1 and 2). Although there is no sapropel present during most of the cycles of the Lower Abad, the middle–upper part of the homogeneous marls below the indurated layers are characterized by extremely abundant warm-oligotrophic planktonic foraminiferal fauna's that are linked to sapropels both in the Upper Abad as well as in Neogene marine successions in the Mediterranean in general (Sierro et al., 1997, 1999). Since sapropels are invariably linked with precession minima in the Mediterranean Neogene, we tuned the middle–upper part of the homogeneous marls with summer insolation maxima. Moreover, the first sapropels recorded from cycle LA17 upwards occur without exception in the middle-upper part of the

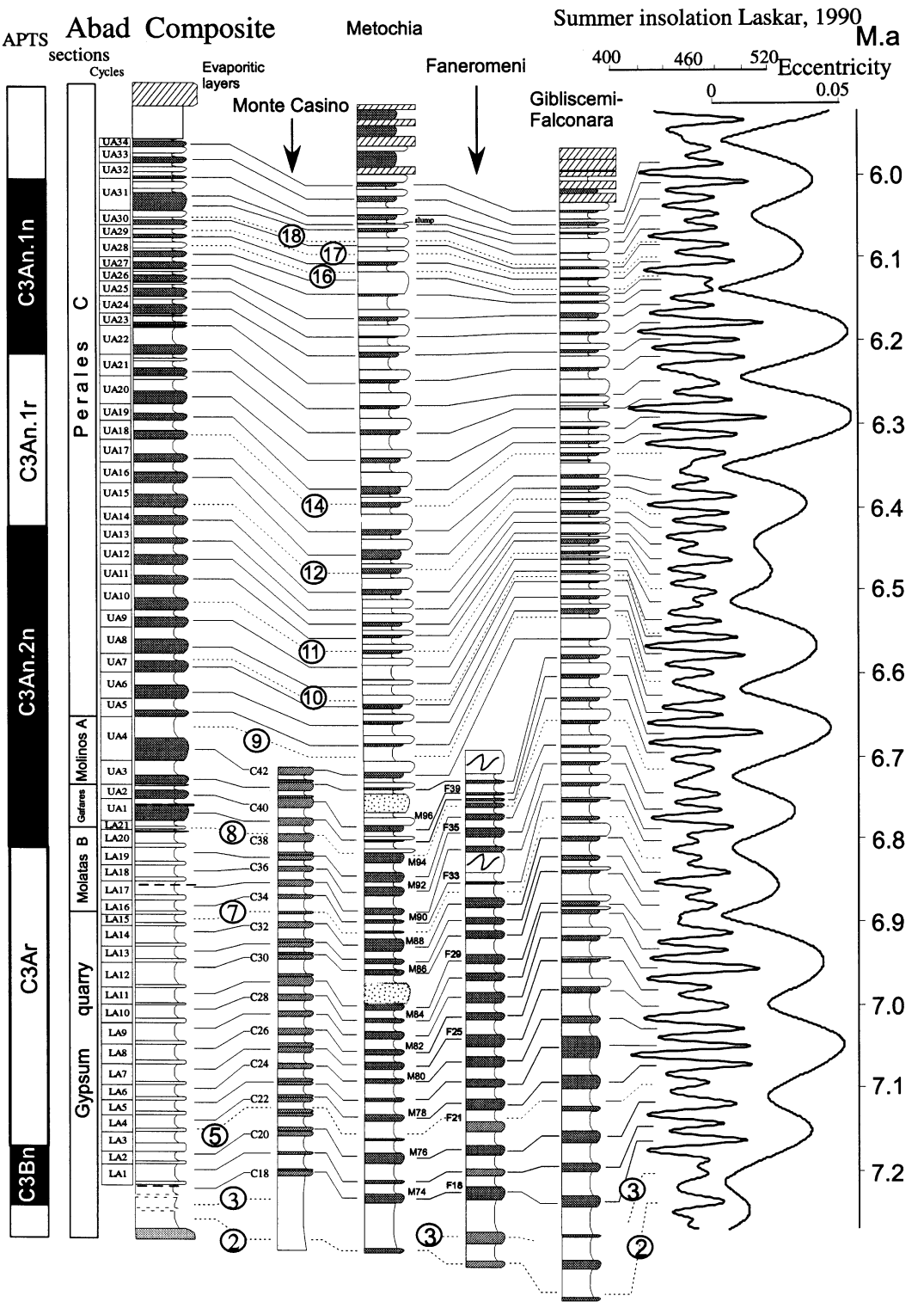
APTS
Abad Composite
sections
Cycles
Evaporitic layers
Monte Casino
Metochia
Faneromeni
Gibliscemi-Falconara
Summer insolation Laskar, 1990
M.a
400
460
520
Eccentricity
0
0.05
C3An.1n
C3An.1r
C3An.2n
C3Ar
C3Bn
Perales
C
Molinos A
Gelfares
Molatas B
Gypsum quarry
6.0
6.1
6.2
6.3
6.4
6.5
6.6
6.7
6.8
6.9
7.0
7.1
7.2

Table 1
Astronomical age of individual sedimentary cycles of the Abad composite. Ages refer to the mid-points of sapropels in the upper abad or mid-point between two indurated layers in the Lower Abad and represent 3-kyr lagged ages of the correlative insolation maxima. The 3-kyr lag is based on the difference in age between the youngest Holocene saproprel in the Mediterranean and the correlative precession minimum/insolation maximum

Sedimentary cycle	*i* Age
UA-34	5.993
UA-33	6.015
UA-32	6.034
UA-31.2	6.053
UA-31.1	6.070
UA-30	6.091
UA-29	6.110
UA-28	6.132
UA-27	6.145
UA-26	6.164
UA-25	6.184
UA-24	6.205
UA-23	6.226
UA-22	6.257
UA-21	6.278
UA-20	6.299
UA-19	6.320
UA-18	6.342
UA-17	6.373
UA-16	6.393
UA-15	6.412
UA-14	6.432
UA-13	6.452
UA-12	6.470
UA-11	6.490
UA-10	6.509
UA-9	6.524
UA-8	6.544
UA-7	6.563
UA-6	6.585
UA-5	6.606
UA-4	6.635
UA-3	6.657
UA-2	6.678
UA-1	6.699
LA-20	6.721
LA-19	6.752
LA-18	6.771
LA-17	6.792
LA-16	6.810
LA-15	6.829
LA-14	6.847
LA-13	6.869
LA-12	6.887
LA-11	6.920
LA-10	6.941
LA-9	6.963
LA-8	6.985
LA-7	7.008
LA-6	7.035
LA-5	7.055
LA-4	7.078
LA-3	7.099
LA-2	7.126
LA-1	7.149

homogeneous marls. The homogeneous marls inmediately below the distinct indurated layer of cycle LA1 are characterized by a pronounced maximum in warm oligotrophic planktonic foraminifera, and correlates well with the first prominent Messinian sapropel in other Mediterranean sections. This layer below cycle LA1 corresponds to the first high amplitude peak in insolation following an interval of low-amplitude fluctuations that corresponds to the interval with no distinct cyclicity at the base of the Abad marls (Fig. 11).

Lower Abad cycle patterns can also be correlated with other Mediterranean sections. The extra-ordinary cycle LA12 correlates well with cycles F29 in the Faneromeni section and C29 at Monte del Casino, and corresponds to a precession cycle with a minimum peak in insolation that apparently lacks sedimentary expression. The homogeneous marls above the indurated beds of cycles LA15 and LA16 are thin

Fig. 11. Correlation of the Abad composite with other Eastern Mediterranean sections and calibration of cycle patterns to the 65°N summer insolation and eccentricity curves of Laskar 1990. Dash lines show bioevent correlations. 2. FrO of the *G. miotumida* group. 3. Influx of the highly conical forms of the *G. miotumida* group. 5. LAO of the group of *G. scitula* sin. 7. Bottom acme of the group of *G. scitula* dex (*G. nicolae*). 8. Top acme group of *G. scitula* dex (*G.nicolae*). 9. FAO of G. Siphonifera. 10. Last influx of the *G. miotumida* group. 11. LrO of the *G. miotumida* gr. 12. First abundant influx of *T. Multiloba*. 14. First abundant influx of dextral Neogloboquadrinids. 16. Influx sinistral Neogloboquadrinids. 17. Short influx of the group of *G. scitula* dex. 18. Influx. sinistral Neogloboquadrinids. (see Fig. 5).

and correlate with the very thin sapropels of cycles M89-90 in section Metochia and with the weakly developed grey marl beds of cycles C33-34 at Monte del Casino (Hilgen et al., 1995; Krijgsman et al., 1997).

7.2. The Upper Abad

The Upper Abad marls can be correlated cyclostratigraphically to the Falconara and Metochia sections (Fig. 11), the bed-to-bed correlations being confirmed by the high-resolution planktonic foraminiferal biostratigraphy (Krijgsman et al., 1999). This consistency cannot be explained other than that these pre-evaporite successions are continuous and not punctuated by hiatuses. Krijgsman et al. (1999) calibrated the pre-evaporite cycles to the astronomical record, using the precession and 65° Nlat summer

Table 2
Astronomical ages of all planktonic foraminifera and calcareous nannoplankton bioevents, polarity reversals and ash layers. Ages have been obtained by linear interpolation of the sedimentation rate between astronomically-dated calibration points. The ages of sapropel mid-points were used as calibration points assuming they represent 3-Kyr lagged ages of the correlative summer insolation maxima. For the Lower Abad where sapropels are not present, we have used the mid-points between two consecutive indurated layers as calibration points

Taxa	Event		Range	Chron	Age
N. acostaensis sinistral gr.	2nd influx	Top	6.077–6.080	C3Anln	6.078
		Bottom	6.080–6.084		6.082
G. scitula gr.	2nd influx	Top	6.098–6.100	C3Anln	6.099
		Bottom	6.104–6.107	C3Anln	6.105
N. acostaensis gr	Dominance sinistral forms	Top	6.107–6.109	C3Anln	6.108
		Bottom	6.138–6.141		6.140
N. acostaensis sinistral	1st influx	Top	6.123–6.125	C3Anln	6.124
		Bottom	6.125–6.127		6.126
G. scitula gr	1st influx	Top	6.285–6.289	C3Anlr	6.287
		Bottom	6.290–6.292		6.291
N. acostaensis dextral gr.	FAO		6.337–6.340	C3Anlr	6.339
N. acostaensis gr	Coiling change	Bottom to top	6.345–6.374	C3Anlr	6.360
N. acostaensis sinistral gr.	Last regular influx		6.378–6.379	C3Anlr	6.378
G. multiloba	FAO		6.413–6.416	C3Anlr	6.415
G. miotumida gr.	LrO		6.503–6.505	C3An2n	6.504
G. miotumida gr	Last influx		6.550–6.553	C3An2n	6.552
G. obesa–G. siphonifera	FAO		6.606–6.620	C3An2n	6.613
G. scitula dex gr. (*G. nicolae*)	Acme	Top	6.713–6.714	C3An2n	6.713
		Bottom	6.827–6.829		6.828
G. scitula dextral gr.	Reduction		7.005–7.008		7.007
G. scitula sinistral gr.	LAO		7.091–7.100		7.095
R. pseudoumbilicus	Top paracme		7.110–7.114		7.112
High conical G. miotumida gr.	1st influx	Top	7.182–7.189		7.186
		Bottom	7.202–7.208		7.205
G. miotumida gr.	FrO		7.239–7.245		7.242
G. menardii dextral gr.	LO		7.257–7.264		7.260

Reversal	Range	Age	CK95	HKLLSZ
C3An.ln (y)	6.031–6.038	6.035	5.875	5.952
C3An.ln. (o)	6.240–6.266	6.253	6.122	6.214
C3An.2n (y)	6.430–6.443	6.437	6.256	6.356
C3An.2n(o)	6.719–6.751	6.735	6.555	6.677

Ash layer	Age
1	6.692
2	6.789
3	7.161

insolation curve of solution $La90_{(1,1)}$ as target. Starting from the previously established astronomical tuning of older cycles of Tortonian and early Messinian age (Hilgen et al., 1995), the younger cycles were in first instance tuned to successively younger insolation maxima/precession minima. The final tuning was only achieved after details of the sedimentary cycle patterns related to eccentricity modulation of precession and interference between precession and obliquity had been taken into account. These patterns are clear in the Metochia and Falconara sections (Hilgen and Krijgsman, 1999 and unpublished data), but although less obvious can also be recognized in the cycle patterns of the Upper Abad.

Both the first, greyish sapropel (of cycle LA17) as well as the first prominent, brownish sapropel (of UA1) correspond to an increase in amplitude of precession and insolation related to the eccentricity modulation of precession. The extra-ordinary thick homogeneous marl of UA4 correlates with a precession cycle having a prolonged 29 kyr period (Fig. 11). The other aberrantly thick homogeneous marl of UA17 does not reflect a longer than average precession cycle but represents a double cycle in which the upper sapropel lacks sedimentary expression (Fig. 11). This missing sapropel correlates with a very low-amplitude peak in precession/insolation connected with modulation by the 100 kyr eccentricity cycle. Also cycle UA31 is interpreted as a double cycle, but in this case the "lower" homogeneous marl is not developed, resulting in the extremely thick sapropel of UA31. Actually, the lower and upper part of this sapropel are faintly laminated in the Los Molinos section whereas the middle part is homogeneous but retains the typical brownish color of the sapropel.

In all sections, the sapropel of cycle UA13 is extremely thin and devoid of the warm oligotrophic fauna typical of sapropels. But also sapropels UA11 and UA9 are thinner than adjacent sapropels in most of the sections (Fig. 11). Such alternating thin–thick–thin–thick patterns reflect interference between precession and obliquity, whereby the thicker sapropels correspond to the more prominent insolation maxima (Hilgen et al., 1995; Lourens et al., 1996). Note, however, that the eccentricity modulation usually play an additional role in determining the exact pattern of the interference (see Hilgen and Krijgsman, 1999).

For cycles UA9–UA13 the correlative interference pattern is easily identified in the insolation record (Fig. 11) and the weakest insolation maximum indeed corresponds to sapropel UA13 (only the insolation maximum at 6.35 Ma is further reduced in amplitude but at that time no sapropel was formed at all as discussed before). Looking at the sapropel thickness pattern, the interference signal may even be extended downward to include sapropels UA4–UA8, but the expected reduction in the amplitude of the insolation maximum that corresponds to sapropel UA7 is not observed in the insolation target.

Interference patterns are also observed in the non-sapropelic parts of the cycles, most prominently so in the thickness pattern of the diatomites in cycles UA26–UA33. The alternating thin–thick pattern exactly matches the interference pattern in the insolation target whereby thicker and more prominent diatomites correspond to high amplitude peaks of, in this case, insolation minima. The homogeneous marls of UA5, UA7, UA9 and UA11 are usually but not always thinner than the homogeneous marls of the adjacent cycles. But in this case the thinner homogeneous marl of cycle UA5 and UA7 do not fit the interference pattern in the insolation minima. Note, however, that the same misfits have been found for exactly the same cycles in the Falconara section on Sicily (Hilgen and Krijgsman, 1999).

As already stated in our paper on the astrochronology of the Tripoli diatomite Formation (Hilgen and Krijgsman, 1999), we assume that the astronomical tuning of the pre-evaporite successions in the Mediterranean is essentially correct despite the observed minor misfits in the interference patterns. A small inaccuracy in the applied astronomical solution provides the most likely explanation for these misfits. Ongoing research directed at improving the accuracy of the astronomical solution may result in minor modifications in the future but will not seriously affect the tuning and, hence, the astrochronology of the Abad marls.

8. Closing the Messinian gap in the astronomical polarity time scale

The APTS for the Plio-Pleistocene is partly based on cyclically-bedded sequences of the Mediterranean

(Hilgen 1991a,b). The APTS proved to be more accurate and has a higher resolution than conventional time scales, and has therefore been incorporated in the standard geomagnetic polarity time scale of Cande and Kent (1995). Recently, the Mediterranean APTS has been extended into the Miocene, based on sections from Crete, Gavdos and Sicily, and covers a time-span from late Serravallian (12.2 Ma) to early Messinian (6.8 Ma) (Hilgen et al., 1995, 2000). Since the Plio-Pleistocene APTS covered the last 5.3 Myr, this resulted in a "Messinian gap" from 5.3 to 6.8 Ma, comprising the paleomagnetic reversals of chron C3An.

The Abad marls are the only cyclically-bedded unit in the Mediterranean that provides a reliable magnetostratigraphy for this interval. Our magnetostratigraphic results from the Upper Abad are consistent with the results of Gautier et al. (1994) and indicate that the normal polarity intervals correspond to the Messinian chrons C3An.1n and C3An.2n of the geomagnetic polarity time scale (Cande and Kent, 1995). The reversed level in the sapropel of cycle UA28 might be a diagenetic artefact, but can also signify a reversed cryptochron in C3An.1n. In this respect it is noteworthy that the magnetostratigraphic record of Hole 845A, of Leg 138 in the eastern equatorial Pacific, also shows anomalous (reversed?) directions in the middle of chron C3An.1n (Schneider, 1995).

Our magnetostratigraphy is confirmed by the position of the coiling change of *N. acostaensis* in the middle of chron C3An.1r, in perfect agreement with the results of Gautier et al. (1994) and with results from DSDP Site 609 of the adjacent Atlantic (Hooper and Weaver, 1987). Tuning of the sedimentary cycle patterns in the Abad marls to insolation results in new astronomical ages for the paleomagnetic reversal boundaries (Table 1), thus closing the Messinian gap in the APTS.

The ages of all four reversals are considerably older than previously reported in the conventional time scales of Cande and Kent (1992, 1995), in the astronomical time scales of Hilgen et al. (1995), Shackleton et al. (1995) and Benson et al. (1995). These considerable divergent ages in the different astronomical time scales can be explained by the fact that the ages of the Hilgen et al. (1995) time scale do not represent true astronomical ages, but ages that were calculated on the basis of linear interpolation of sea floor spreading rates using astronomical ages for the next younger and older reversal as calibration points. The Shackleton et al. (1995) time scale was a first preliminary attempt to establish a partial astronomical tuning for ODP leg 138 records in the interval between 6 and 10 Ma. Detailed quantitative analysis of calcareous nannofossils, however, suggests that the preliminary astronomical tuning for leg 138 is not correct, but that revised ages are in perfect agreement with the results from our Spanish sections (Krijgsman et al., 1999). The older ages for chron C3An are further supported by their implication for sea floor spreading rates which appear to give the simplest picture with the new astronomical ages (see also Krijgsman et al., 1999). Finally, we also investigated the Ain el Beida section used by Benson et al. (1995) to obtain astronomical ages for the C3An.1n reversals. Our preferred tuning for the sedimentary cycles in this section is at odds with that of Benson et al. (1995) and will be presented in a forthcoming paper.

The quoted error estimates in our astronomical ages for the reversals do not refer to the potential error in the astronomical dating but to the uncertainty in the exact (stratigraphic) position of the magnetic polarity reversals with respect to the astronomically-dated cycles. Unfortunately, the exact error in the astronomical solution and, hence, in our astronomical ages cannot be exactly calculated due to the complexity of the solution. As a consequence, no statistically computed errors can be added to astronomical ages although they can be assumed to be very small (in the order of ± 0.003 Myr; see also Quinn et al., 1991), providing that the tuning itself is correct. The astronomical ages of sedimentary cycles and bioevents simply refer to the exact astronomical age of the corresponding peak in the insolation time series according to the applied astronomical solution.

9. Calcareous plankton astrobiochronology for the Mediterranean Messinian

The astronomical tuning of the sedimentary cycles in addition provided accurate ages for the calcareous plankton bioevents in the Abad composite. Comparison of these ages with astronomical ages obtained for the same events in other sections located throughout

the Mediterranean will reveal whether these events are synchronous on a Mediterranean scale.

9.1. The Lower Abad

The FRO of the *G. miotumida* group is recorded in the non-cyclic basal interval of the Lower Abad and is astronomically dated at 7.242 Ma (Table 2). This event is immediately preceeded by the LO of the group of *G. menardii* 5 and is a well known event usually cited in the Mediterranean as the FRO of the *G. conomiozea* group (Zachariasse, 1975, 1979a,b; D'Onofrio et al., 1975; Iaccarino et al., 1975; Bossio et al., 1976; Gonzalez Donoso and Serrano, 1977; Cita and Ryan, 1978; Glaçon et al., 1990; Sierro et al., 1993, 1997; Krijgsman et al., 1994, 1995, 1997). The FRO of the *G. conomiozea* group, with an astronomical age of 7.24 Ma (Hilgen et al., 1995), has been widely used as a biostratigraphic indicator for the Tortonian/Messinian boundary. The event has also been recognised in the Northeast Atlantic (Feinberg and Lorenz, 1970; Bossio, 1976; Cita and Ryan, 1978; Sierro, 1985; Sierro et al., 1993; Hodell et al., 1989; Benson et al., 1991). Unlike the Mediterranean, where these groups have never been found coexisting (with the exception of the Potamida section on Crete; Zachariasse, 1979b), the *G. menardii* group is clearly replaced by the *G. miotumida* group after a short period of coexistence in the Atlantic (Sierro, 1985; Sierro et al., 1993). Although the Lower Abad did not produce reliable magnetostratigraphic data, this event has been pinpointed in a reversed interval corresponding to subchron C3Br.1r in the Kastelli and Faneromeni sections on Crete and the Metochia section on Gavdos (Krijgsman et al., 1994, 1995, 1997). Moreover, the influx of highly conical types of the *G. miotumida* group, located $1\frac{1}{2}$ cycles below cycle LA1 in the Abad composite, can be correlated with the influx of *G. conomiozea* s.s., identified below sapropel C18 at Monte del Casino (Northern Italy) and below the first sapropel in the Potamida section (Crete) with an astronomical age of 7.19 Ma (Krijgsman et al., 1997).

The top of the *R. pseudoumbilicus* paracme has been widely used as a globally synchronous event recorded in the Indian, Pacific and Atlantic Oceans (Rio et al., 1990; Raffi and Flores, 1995; Backman and Raffi, 1997). In the Abad sections this bioevent has been located at the limit between cycles LA2 and LA3 with an astronomical age of 7.112 Ma. This event is positioned very close to the paleomagnetic reversal C3Bn(y) in Eastern Mediterranean sections (Krijgsman et al., 1995). Raffi and Flores (1995) recorded the top of this paracme close to the onset of Chron C3Ar in the Eastern Equatorial Pacific. The same event was dated by Backman and Raffi (1997) at 7.1 Ma at ODP Site 926 (Ceara Rise) using the astronomical time scale of Shackleton and Crowhurst (1997). Although paleomagnetic data were not retrieved from this hole, the age assignment is in good agreement with the age of the C3Bn/C3Ar reversal according to the astronomical time scale of Hilgen et al. (1995).

The LAO of the sinistral forms of the *G. scitula* group is located in cycle LA3 in Sorbas and dated at 7.095 Ma. The same event has been identified in cycle C21 of the Monte del Casino section (Krijgsman et al., 1997) and in the Metochia and Faneromeni sections (unpublished data). The strong reduction in abundance of dextral specimens of the *G. scitula* group is recorded in cycle LA7, dated at 7.007 Ma. The acme of the dextral forms of the *G. scitula* group (morphotype *G. nicolae*) is found between cycles LA15 and LA20 (6.828–6.71 Ma) in Sorbas and correlates well with the same acme recorded between C33 and C38 at Monte del Casino. The base of the *G. nicolae* acme has an astronomical age of 6.82 Ma in the Metochia and Faneromeni sections (Hilgen et al., 1995).

9.2. The Upper Abad

The FAO of *G. siphonifera/G. obesa* morphotypes is located within cycle UA4 in all sections in the Nijar and Sorbas basins and is astronomically dated at 6.613 Ma. The same event has also been identified in Metochia and Gibliscemi/Falconara (unpublished data). Sprovieri et al. (1996b) identified a prominent peak of *G. siphonifera* at exactly the same cycle (8.5 cycles above the FO of *G. nicolae*) at Monte Gibliscemi.

The LO of the *G. miotumida* group is recorded within cycle UA10 with an age of 6.504 Ma and can be traced to the Central (Falconara–Gibliscemi sections) and Eastern Mediterranean (Metochia section) (Krijgsman et al., 1999; Hilgen and Krijgsman, 1999). This event occurs in the upper part of chron C3An.2n and is useful for Mediterranean-wide correlations. It is older, however, than the same bioevent in the North Atlantic, where it has

been recorded immediately after the first coiling change of the neogloboquadrinids (see Sierro, 1985; Sierro et al., 1993; Hodell et al., 1994; Zhang and Scott, 1996) within chron C3An.1r. The progressively restricted connection between the Atlantic and Mediterranean during the Messinian is probably responsible for the earlier disappearance of this species from the Mediterranean.

Some of the short influxes of keeled and unkeeled globorotaliids, such as the last two abundant influxes of the *G. miotumida* group occurring in cycles UA6 and UA7 (6.552 Ma) or the influxes of *G. scitula* located in cycles UA20 (6.289 Ma) and UA29 (6.103 Ma), have also been recognised elsewhere in the Mediterranean (Falconara section, Hilgen and Krijgsman, 1999; Metochia section (unpublished data).

The first occurrence of *T. multiloba* has been widely used for biostratigraphic correlations inside the Mediterranean. D'Onofrio et al. (1995) used the FAD of this species to define the base of the *T. multiloba* subzone located immediately above the first coiling change in *Neogloboquadrina acostaensis*. Iaccarino et al. (1985) also reported this species inside a non-distinctive zone above the coiling change in Neogloboquadrinids. More recently, Sprovieri et al. (1996a,b) reported that this species first occurs three lithological cycles above the coiling change in neogloboquadrinids on Sicily. Here we prefer to use the FAO of *T. multiloba* which has also been identified in the Falconara/Gibliscemi and Metochia sections at equivalent levels (Krijgsman et al., 1999; Hilgen and Krijgsman, 1999; unpublished data). This bioevent has been recorded 3 cycles below the first coiling change in the Neogloboquadrinids and is dated astronomically at 6.415 Ma.

The sinistral-to-dextral coiling change in neogloboquadrinids occurs in cycle UA17 with an astronomical age of 6.361 Ma. This event has frequently been recognised both in the Mediterranean (Zachariasse, 1975; Montenat et al., 1976; Civis et al., 1979; Iaccarino, 1985; Van de Poel, 1991; Sierro et al., 1993, 1997; Gautier et al., 1994; Sprovieri et al., 1996a,b) and in the Atlantic (Feinberg and Lorenz, 1970; Bossio et al., 1976; Cita and Ryan, 1978; Salvatorini and Cita, 1979; Sierro, 1984, 1985; Sierro et al., 1993; Hodell et al., 1989; Benson et al., 1991; Zhang and Scott 1996). Iaccarino (1985) used this event to define the base of the non-distinctive zone in the Mediterranean. In the Abad composite, the event lies in the middle of Chron C3An.1r which fits well with magnetostragraphic calibrations in the North Atlantic (Hooper and Weaver 1987; Hodell et al., 1991). Although the coiling change in neogloboquadrinids is often used for biostratigraphic correlations, it occurred at a time when the neogloboquadrinids were rare in the Mediterranean. We thus consider that the first abundant incursion of dextral neogloboquadrinids within cycle UA18 (6.339 Ma) is a more reliable and easily identifiable event. This event has also been identified in Metochia and Gibliscemi/Falconara (Krijgsman et al., 1999; Hilgen and Krijgsman, 1999; unpublished data).

Above this event, the dextral Neogloboquadrinids are dominant, but two new incursions of sinistral forms are found in cycles UA28 and UA30 dated at 6.126 and 6.082 Ma. These incursions are also very reliable for Mediterranean correlations, since they have been observed in the correlative cycles in the central and eastern Mediterranean (Krijgsman et al., 1999; Hilgen and Krijgsman, 1999; unpublished data). Both events are located in the middle part of chron C3An.1n.

Finally, our high-resolution quantitative data indicate that variations in the abundances of specific taxa can be correlated across the Mediterranean as well. For example the interval between the top of cycle UA12 and cycle UA14 dominated by *G. bulloides* has been also recognised in the Falconara and Metochia sections (Hilgen and Krijgsman, 1999; unpublished data).

10. Conclusions

Our cyclostratigraphic, biostratigraphic and magnetostratigraphic study of several partly overlapping sections allows the construction of a composite section for the Abad marls in the Sorbas and Nijar basins in SE Spain. The Abad Composite contains a continuous marine succession from the Tortonian/Messinian boundary up to the evaporites of the Messinian salinity crisis and is perfectly suitable to establish an astronomical (polarity) time scale for the pre-evaporitic Messinian in the Mediterranean.

Cyclostratigraphic correlations to other Mediterranean sections are straightforward and confirmed by the high-resolution biostratigraphy. Eighteen biostratigraphic events are recognised which are useful for

Mediterranean-wide correlations. The cyclostratigraphic position of all magnetic reversals of chron C3An could be reliably determined although the paleomagnetic signal is admittedly weak. Astronomical tuning of the sedimentary cycles to the insolation curve of $La90_{(1,1)}$ provides accurate ages for all cycles, bioevents, ash layers and magnetic reversals, resulting in a high-resolution calcareous plankton astrobiochronology and the closure of the Messinian gap in the APTS.

Acknowledgements

This research is partly supported by DGCYES projects PB98-0268, Fulbright Program and Fundación Ramón Areces in Spain and partly by the The Netherlands Geosciences Foundation (GOA) with financial aid from the Netherlands Organisation of Scientific Research (NWO). Critical reviews of E.McClelland and R.H. Benson are acknowledged. Thanks are due to Jesús Roncero for technical assistance in sample processing.

References

Backman, J., Raffi, I., 1997. Calibration of Miocene Nannofossil events to orbitally tuned cyclostratigraphies from Ceara Rise. Proc. ODP, Sci. Results 154, 83–99.

Benson, R.H., Hayek, L.A., Modell, D.A., Rakic-El Bied, K., 1995. Extending the climate precision curve back into the late Miocene by signature template comparison. Paleoceanography 19, 5–20.

Benson, R.H., Rakic El Bied, K., Bonaduce, G., 1991. An important current reversal (influx) in the rifain corridor (Morroco) at the Tortonian–Messinian boundary: the end of the Tethys ocean. Paleoceanography 6 (1), 164–172.

Bossio, A., El-Bied Rakic, K., Giannelli, L., Mazzei, R., Russo, A., Salvatorini, G., 1976. Correlation de quelques sections stratigraphiques du Mio-Pliocene de la zone atlantique du Maroc avec les stratotypes du bassin Mediterraneen sur la base des foraminiferes planctoniques, nannoplancton calcaire et ostracodes. Atti. Soc. Tosc. Sci. Nat. Mem. 83, 121–137.

Braga, J.C., Martin, J.M., 1996. Geometries of reef advance in response to relative sea-level changes in a Messinian (uppermost Miocene) fringing reef (Cariatiz reef, Sorbas basin, SE Spain). Sediment. Geol. 107, 61–81.

Cande, S.C., Kent, D.V., 1992. A New Geomagnetic Polarity Time Scale for the late Cretaceous and Cenozoic. J. Geophys. Res. 13, 13917–13951.

Cande, S.C., Kent, D.V., 1995. Revised calibration of the geomagnetic polarity time scale for the Late Cretaceous and Cenozoic. J. Geophys. Res. 100, 6093–6095.

Cita, M.B., Ryan, W.B.F., 1978. The Bou Regreg section of the Atlantic coast of Morocco, evidence, timing and significance of a late Miocene regressive phase. Riv. Ital. Paleontol. 84 (4), 1051–1082.

Civis, J., Martinell, J., de Porta, J., 1979. Microfauna del Mioceno terminal de la Rambla de Arejos (Almeria). Studia Geol. 15, 37–55.

Clauzon, G., Suc, J.P., Gautier, F., Berger, A., Loutre, M.F., 1996. Alternate interpretation of the Messinian salinity crisis: Controversy resolved? Geology 24, 363–366.

Colalongo, M.L., Di Grande, A., D'Onofrio, S., Giannelli, L., Iaccarino, S., Mazzei, R., Romeo, M., Salvatorini, G., 1979. Stratigraphy of Late Miocene Italian sections straddling the Tortonian–Messinian boundary. Boll. Soc. Pal. Ital. 18 (2), 258–302.

Dabrio, C.J., Martín, J.M., Megías, A.G., 1985. The tectosedimentary evolution of Mio-Pliocene reefs in the province of Almería. In: Milá, M.D. Rosell, J. (Eds.), 6th European Regional Meeting of Sedimentologists, Excursion Guidebook. Lleida, pp. 104–107.

Dronkert, H., Pagnier, H., 1997. Introduction to the Mio/Pliocene of the Sorbas basin. Messinian Seminar, 3. Field Trip No. 2, 1–21.

Feinberg, H., Lorenz, H.G., 1970. Nouvelles données stratigraphiques sur le Miocène superieur et le Pliocène de Maroc nord-occidentale. Notes Serv. Geol. Maroc 30, 21–26.

Gautier, F., Clauzon, G., Suc, J.P., Cravatte, J., Violanti, D., 1994. Age et duree de la crise de salinite messinienne. , Comptes Rendus, ser. 2, vol. 318. Academie des Sciences (pp. 1103–1109).

Geerlings, L.P.A. 1977. Planktonic foraminifera of the Abad member (Messinian). Turre formation, in the Sorbas basin (Almeria, SE Spain). UNESCO–IUGS. IGCP. Project no. 96. Messinian Correlation. Messinian Seminar no. 3. Excursion no. 2, pp. 37–43.

D'Onofrio, S., Giannelli, L., Iaccarino, S., Morlotti, E., Romeo, M., Salvatorini, G., Sampo, M., Sprovieri, R., 1975. Planktonic foraminifera of the upper Miocene from some Italian sections and the problem of the lower boundary of the Messinian. Boll. Soc. Paleontol. Ital. 14 (2), 177–196.

Glaçon, G., Vergnaud Grazzini, C., Iaccarino, S., Rehault, J.P., Randrianasolo, A., Sierro, F.J., Weaver, P.P.E. 1990. Planktonic foraminiferal events and stable isotopic record in the upper miocene of the Tyrrhenian Sea, ODP site 654, Leg 107. In: Kastens, K.A., Mascle, J. et al. (Eds.), Proceedings of the Ocean Drilling Program, Scientific Results, vol. 107, pp. 415–427.

Gonzalez Donoso, J.M., Serrano, F., 1977. Bio y cronoestratigrafia de los materiales pre-evaporiticos de Sorbas (provincia de Almeria). Messinian Seminar, vol. 3, excursion 2 (Sorbas), pp. 69–76.

Hilgen, F.J., 1987. Sedimentary rhythms and high resolution chronostratigrapic correlations in the Mediterranean Pliocene. Newsl. Stratigr. 17, 109–127.

Hilgen, F.J., 1991a. Astronomical calibration of Gauss to Matuyama sapropels in the Mediterranean and implication for the Geomagnetic Polarity Time Scale. Earth Planet. Sci. Lett. 104, 226–244.

Hilgen, F.J., 1991b. Extension of the astronomically calibrated (polarity) time scale to the Miocene/Pliocene boundary. Earth Planet. Sci. Lett. 107, 349–368.

Hilgen, F.J., Krijgsman, W., 1999. Cyclostratigraphy and astrochronology of the Tripoli diatomite Formation (pre-evaporite Messinian, Sicily, Italy). Terra Nova 11, 16–22.

Hilgen, F.J., Krijgsman, W., Langereis, C.G., Lourens, L.J., Santarelli, A., Zachariasse, W.J., 1995. Extending the astronomical (Polarity) time scale into the Miocene. Earth Planet. Sci. Lett. 136, 495–510.

Hilgen, F.J., Krijgsman, W., Raffi, I., Turco, E., Zachariasse, W.J., 2000. Integrated stratigraphy and astronomical calibration of the Serravallian/Tortonian boundary section at Monte Gibliscemi (Sicily, Italy). Mar. Micropal. 38, 181–211.

Hodell, D.A., Benson, R.H., Kennett, J.P., Rakic-El Bied, 1989. Stable isotope stratigraphy of Late Miocene–Early Pliocene sequences in Northwest Morocco: the Bou Regreg Section. Paleoceanography 4 (4), 467–482.

Hodell, D.A., Benson, R.H., Kent, D.V., Boersma, A., Rakic-El Bied, K., 1994. Magnetostratigraphic, biostratigraphic, and stable isotope stratigraphy of an upper Miocene drill core from Salé Briqueterie (Northwestern Morocco). A high resolution chronology for the Messinian stage. Paleoceanography 9, 835–855.

Hooper, P.W.P., Weaver, P.P.E. 1987. Paleoceanographic significance of Late Miocene to Early Pliocene planktonic foraminifers at Deep Sea Drilling Project Site 609. Initial Rep. Deep Sea Drill. Proj. 94, pp. 925–934.

Iaccarino, S., 1985. Mediterranean Miocene and Pliocene Planktic foraminifera. In: Bolli, H.M., Saunders, J.B., Perch-Nielsen, K. (Eds.), Plankton Stratigraphy. Cambridge University Press, pp. 283–314.

Iaccarino, S., Morlotti, E., Papani, G., Pelosio, G., Raffi, S., 1975. Litostratigrafia e biostratigrafia di alcune serie neogeniche della provincia de Almeria. Ateneo parmense. Acta Nat. 11, 237–313.

Kirschvink, J.L., 1980. The least-squares line and plane and the analysis of paleomagnetic data. Geophys. J. R. Astron. Soc. 62, 699–718.

Krijgsman, W., 1996. Miocene magnetostratigraphy and cyclostratigraphy in the Mediterranean: extension of the astronomical polarity time scale. Geologica Utraiectina. 141, 207 pp.

Krijgsman, W., Hilgen, F., Langereis, C.G., Zachariasse, W.J., 1994. The age of the Tortonian/Messinian boundary. Earth Planet Sci. Lett. 121, 533–547.

Krijgsman, W., Hilgen, F.J., Langereis, C.G., Santarelli, A., Zachariasse, W.J., 1995. Late Miocene magnetostratigraphy, biostratigraphy and cyclostratigraphy in the Mediterranean. Earth Planet. Sci. Lett. 136, 475–494.

Krijgsman, W., Hilgen, F.J., Negri, A., Wijbrans, J.R., Zachariasse, W.J., 1997. The Monte del Casino section (Northern Apennines, Italy): a potential Tortonian/Messinian boundary stratotype? Palaeogeogr. Palaeoclimatol. Palaeoecol. 133, 27–47.

Krijgsman, W., Hilgen, F.J., Raffi, I., Sierro, F.J., Wilson, D.S., 1999. Messinian astrochronology and the synchroneity of the salinity crisis. Nature 400, 652–655.

Langereis, C.G., Dekkers, M.J., 1992. Paleomagnetism and rock magnetism of the Tortonian–Messinian boundary stratotype at Falconara, Sicily. Phys. Earth Plan. Int. 71, 100–111.

Langereis, C.G., Hilgen, F.J., 1991. The Rossello composite: A mediterranean and global reference section for the early to early–late Pliocene. Earth Planet. Sci. Lett. 104, 211–225.

Laskar, J., 1990. The chaotic motion of the solar system: a numerical estimate of the size of the chaotic zones. Icarus 88, 266–291.

Lourens, L.J., Antonarakou, A., Hilgen, F.J., Van Hoof, A.A.M., Vergnaud-Grazzini, C., Zachariasse, W.J., 1996. Evaluation of the Pliocene to early Pleistocene astronomical time scale. Paleoceanography 11, 391–413.

Lowrie, W., 1990. Identification of ferromagnetic minerals in a rock by coercivity and unblocking temperature properties. Geophys. Res. Lett. 17, 159–162.

Martin, J.M., Braga, J.C., 1990. Arrecifes messinienses de AlmerÍa. TipologÍas de crecimiento, posición estratigráfica y relación con las evaporitas. Geogaceta 7, 66–68.

Martin, J.M., Braga, J.C., 1994. Messinian events in the Sorbas basin of Southeastern Spain and their implications of the recent history of the Mediterranean. Sediment. Geol. 90, 257–268.

Martin, J.M., Braga, J.C., 1996. Tectonic signals in the Messinian stratigraphy of the Sorbas basin (Almeria, SE Spain). In: Friend, P.F., Dabrio, C.J. (Eds.), Tertiary Basins of Spain, the Stratigraphic Record of Crustal Kinematics. Cambridge University Press, Cambridge, pp. 387–391.

McClelland, E., Finegan, B., Butler, R., 1997. A magnetostratigraphic study of the onset of the Mediterranean Messinian salinity crisis: Caltanissetta Basin, Sicily. Spec. Publ. Geol. Soc. Lond.

Montenat, Ch., Ott d'Estevou, P., 1996. Late Neogene basins evolving in the Eastern Betic transcurrent fault zone: an illustrated review. In: Friend, P.F., Dabrio, C.J. (Eds.). Tertiary Basins of Spain, the StratigrAphic Record of Crustal Kinematics. Cambridge University Press, Cambridge, pp. 372–386.

Montenat, Ch., Bizon, G., Bizon, J.J., 1976. Continuite ou discontinuite de sedimentation marine Mio-Pliocene en Mediterranee occidentale. Inst. Francais du Petrole Revue 31, 613–663.

Müller, D.W., Hsü, K.J., 1987. Event stratigraphy and paleoceanography in the Fortuna basin (Southeast Spain): A scenario for the Messinian Salinity Crisis. Paleoceanography 2 (6), 679–696.

Negri, A., Vigliotti, L., 1997. Calcareous nannofossil biostratigraphy and paleomagnetism of the Monte Tondo and Monte del Casino sections (Romagna Appennine). In: Montanari, A., Odini, G.S., Coccioni, R. (Eds.), Miocene Stratigraphy: An Integrated Approach. Elsevier Science, Amsterdam, pp. 477–491.

Ott d'Estevou, P., 1980. Evolution dynamique du bassin neogène de Sorbas (Cordillères Bétiques Orientales. Espagne). Docum. et Trav. IGAL., vol. 1, 264 pp.

Quinn, T.R., Termain, S., Duncan, M., 1991. A three million year integration of the Earth's orbit. Astron. J. 101, 2287–2305.

Raffi, I., Flores, J.A., 1995. Pleistocene through Miocene calcareous nannofossils from eastern equatorial Pacific Ocean (Leg 138). In: Pisias, N.G., Mayer, L.A., Janecek, T.R., Palmer Hulson, A., Van Andel, T.H., (Eds.), Proc. ODP, Sci. Results, 138: College Station, TX (Ocean Drilling Program), pp. 233–286.

Riding, R., Braga, J.C., MartÍn, J.M., Sánchez-Almazo, I.M., 1998.

Mediterranean Messinian Salinity Crisis: constraints from a coeval marginal basin, Sorbas, southeastern Spain. Marine Geology 146, 1–20.

Riding, R., Braga, J.C., MartÍn, J.M., 1999. Late Miocene Mediterranean desiccation: topography and significance of the 'Salinity Crisis' erosion surface on-land in southeast Spain. Sediment. Geol. 123 (1–2), 1–7.

Rio, D., Fornaciari, E., Raffi, I., 1990. Late Oligocene through early Pleistocene calcareous nannofossils from western equatorial Indian Ocean (Leg 115). Proc. ODP, Sci. Results 115, 175–235.

Ruegg, G.J.H., 1964. Geologische onderzoekingen in het bekken van Sorbas, S Spanje. Amsterdam Geological Institut, University of Amsterdam, 64 pp.

Salvatorini, G., Cita, M.B., 1979. Miocene Foraminiferal stratigraphy DSDP site 397 (Cape Bojador, North Atlantic). Initial Reports of the Deep Sea Drilling Project vol. 47 (1), pp. 317–375.

Schneider, D.A., 1995. Paleomagnetism of some leg 138 sediments: detailing Miocene magnetostratigraphy. Proc. ODP, Sci. Results 138, 59–72.

Shackleton, N.J., Crowhurst, S., 1997. Sediment fluxes based on an orbitally tuned time scale 5 Ma to 14 Ma, Site 926. Proc. ODP, Sci. Results 154, 69–82.

Shackleton, N.J., Crowhurst, S., Hagelberg, T., Pisias, N.G., Schneider, D.A., 1995. A new late Neogene time scale: Application to leg 138 sites. Proc. ODP Sci. Results 138, 73–101.

Sierro, F.J., 1984. ForaminÍferos planctónicos y biostratigrafÍa del Mioceno superior del borde occidental de la cuenca del Guadalquivir (S.O de España). Tesis Doctorado. Universidad de Salamanca, 391 pp.

Sierro, F.J., 1985. The replacement of the "Globorotalia menardii" group by the Globorotalia miotumida group: an aid to recognizing the Tortonian/Messinian boundary in the Mediterranean and adjacent Atlantic. Mar. Micropaleontol. 9 (6), 525–535.

Sierro, F.J., Flores, J.A., Civis, J., González Delgado, J.A., Francés, G., 1993. Late Miocene globorotaliid event-stratigraphy and biogeography in the NE Atlantic and Mediterranean. Mar. Micropaleontol. 21, 143–168.

Sierro, F.J., Flores, J.A., Zamarreño, I., Vazquez, A., Utrilla, R., Francés, G., Hilgen, F., Krijgsman, W., 1997. Astronomical cyclicity and sapropels in the pre-evaporitic Messinian of the Sorbas basin (Western Mediterranean). Geogaceta 21, 131–134.

Sierro, F.J., Flores, J.A., Zamarreño, Y., Vazquez, A., Utrilla, R., Francés, G., Hilgen, F.J., Krijgsman, W., 1999. Messinian pre-evaporite sapropels and precession-induced oscillations in western Mediterranean climate. Mar. Geol. 153, 137–146.

Sprovieri, R., Di Stefano, E., Sprovieri, M., 1996a. High resolution chronology for Late Miocene Mediterranean stratigraphic events. Riv. Ital. Pal. 102, 77–104.

Sprovieri, R., Di Stefano, E., Caruso, A., Bonomo, S., 1996b. High resolution stratigraphy in the Messinian Tripoli Formation in Sicily. Paleopelagos 6, 415–435.

Van Hoof, A.A.M., Van Os, B.J., Rademakers, J.G., Langereis, C.G., De Lange, G.J., 1993. A paleomagnetic and geochemical record of the upper Cochiti reversal and two subsequent precessional cycles from southern Sicily (Italy). Earth Planet. Sci. Lett. 117, 235–250.

Van de Poel, H.M., 1991. Messinian stratigraphy of the Nijar basin (S. E. Spain) and the origin of its gypsum-ghost limestones. Geol. Mijnb. 70, 215–234.

Vazquez, A., Utrilla, R., Zamarreño, Y., Sierro, F.J., Flores, J.A., Francés, G., Barcena, M.A., 2000. Precession related sapropelites of the Messinian Sorbas basin (South Spain): Paleoenvironmental significance. Palaeogeogr. Palaeoclimatol, Palaeoecol. 158 (3–4), 353–370.

Völk, H.R., Rondeel, H.E., 1964. Zur gliederung des Jungtertiars in bechen von Vera, Südost Spanien. Geol. Mijnb. 43, 310–315.

Weijermars, R., Roep, Th.B., Van den Eeckhout, B., Postma, G., Kleverlaan, K., 1985. Uplift history of a batic fold nappe inferred from Neogene Quaternary sedimentation and tectonics (in the sierra alhamilla and Almeria, Sorbas and Tabernas Basins of the Betic Cordilleras, SE Spain). Geol. Mijn. 64, 379–411.

Zachariasse, W.J., 1975. Planktonic foraminiferal biostratigraphy of the Late Neogene of Crete (Greece). Utrecht Micropal. Bull., 11.

Zachariasse, W.J. 1979a. The origin of *Globorotalia conomiozea* in the Mediterranean and the value of its entry level in biostratigraphic correlations. Ann. Geol. Pays Hellen., Tome hors serie, fasc. III, VIIth International Congress on Mediterranean Neogene, Athens, pp. 1281–1292.

Zachariasse, J.W., 1979b. Planktonic foraminifera from section Potamidha1: taxonomic and philetic aspects of keeled globorotaliids and some paleoenvironmental estimates. Utrecht Micropal. Bull. no. 21, pp. 129–166.

Zhang, J., Scott, D.B., 1996. Integrated stratigraphy and paleoceanography of the Messinian (Latest Miocene) across the North Atlantic Ocean. Mar. Micropaleontol. 29, 1–36.

Zijderveld, J.D.A., 1967. Demagnetization of rocks: analysis of results. In: Collinson, D.W. (Ed.), Methods in Paleomagnetism. Elsevier, New York, pp. 254–286.